Check for updates

In situ Lu–Hf geochronology with LA-ICP-MS/MS analysis†

Shitou Wu, [ID] ab Hao Wang, [ID] *ab Yueheng Yang, [ID] *ab Junlong Niu,ab Zhongwu Lan, [ID] ab Liangliang Zhang, [ID] c Chao Huang, [ID] ab Liewen Xie, [ID] ab Lei Xu, [ID] ab Jinhui Yangab and Fuyuan Wuab

Lu–Hf geochronology is useful for constraining the evolution of geological systems. In this study, the *in situ* LA-ICP-MS/MS Lu–Hf dating technique was successfully applied to Paleozoic-Precambrian xenotime, apatite and garnet. For an iCap TQ ICP-MS/MS instrument (Thermo Fisher, USA), high-purity NH_3 was more effective in the reaction than the commonly used $1:9$ NH_3–He mixture, and an 80% improvement in sensitivity was achieved using an N_2 flow rate of 4.0 mL min⁻¹. Lutetium, Yb and Hf reaction products with NH_3 were identified in the mass range from 175–300 amu. The reaction product of $^{(176+82)}$Hf (expressed for ^{176}Hf$(^{14}N^1H)(^{14}N^1H_2)(^{14}N^1H_3)_3$, mass shift by +82) is measured for the separation of ^{176}Hf from ^{176}Lu and ^{176}Yb. Isobaric interferences ^{176}Lu and ^{176}Yb have extremely low reaction rates of ~0.0034% and ~0.00036% (at mass shift +82), which are only required to be corrected for the samples (*e.g.*, xenotime) with extremely high ^{175}Lu/^{177}Hf and ^{172}Yb/^{177}Hf ratios. A matrix-induced bias of ^{176}Lu/^{177}Hf ratios was observed between NIST SRM 610 and the samples, which required further correction using matrix-matched reference materials. For xenotime, the accuracy of the common-Hf corrected single-spot ages is generally better than 1.5%, comparable to those obtained by *in situ* U–Pb analysis. The precisions of common-Hf corrected single-spot ages were in a range of 1.5–8.1% and 9.2–36.0% for xenotime and apatite samples. For garnet, the analytical uncertainties of the isochron ages are in a range of 3.5–10%, which could be further improved using a sensitivity-enhanced instrument and/or enlarged sampling volume. Our study revealed that the xenotime reference materials can be used as calibrators for apatite Lu–Hf dating. The novel *in situ* Lu–Hf dating technique may be especially useful for determining the age of the samples with complex temporal records or lack of traditional U-rich accessory minerals (*e.g.*, zircon).

1 Introduction

Lu–Hf geochronology is a powerful technique to constrain the temporal evolution of geological systems, in which ^{176}Lu decays *via* β decay to ^{176}Hf with a half-life of ~37.12 Ga.[1,2] Isochron dating is based on variations in ^{176}Hf contents due to radioactive decay and on the Lu/Hf ratios in rocks and minerals. The first investigation of the Lu–Hf system in geo-and cosmo-chemistry appeared in the early 1980s,[3,4] and the system has been successfully applied to high Lu/Hf phases (*e.g.*, xenotime, apatite, garnet and lawsonite) from a wide variety of magmatic and metamorphic rocks.[5–7] This dating method traditionally requires

time-consuming chemical separation of the parent (^{176}Lu) and decay-product (^{176}Hf) isotopes followed by thermal-ionization mass spectrometry (TIMS) or multicollector-inductively coupled plasma-mass spectrometry (MC-ICP-MS) isotopic measurements,[4,8,9] which is commonly accompanied by a loss of textural context of the analyzed minerals. The presence of accessory phases (*e.g.*, zircon, apatite, monazite or allanite) as inclusions in the target minerals may affect the Lu–Hf systems in different ways. Texturally controlled micro-milling and laser cutting techniques have been suggested for improving spatial resolution and reducing the inclusion effects and successfully applied to mm-size garnet.[10,11] However, it still does not match up to the <100 μm diameter and sub-micron depth resolution like in *in situ* U–Pb dating by using an ion microprobe and laser ablation ICP-MS.

The use of tandem MS with ICP (ICP-MS/MS), where one reaction cell is sandwiched between two quadrupoles, has the potential for online separation of ^{176}Hf from ^{176}Lu and ^{176}Yb isobaric interferences using NH_3 as the reaction gas and analysis of higher–mass reaction products (^{176}Hf$(^{14}N^1H)(^{14}N^1H_2)$ $(^{14}N^1H_3)_3^+$, mass shift by +82).[12] ICP-MS/MS combined with LA micro-sampling has the advantage of rapidly and visually

aState Key Laboratory of Lithospheric Evolution, Institute of Geology and Geophysics, Chinese Academy of Sciences, Beijing, 100029, P. R. China. E-mail: wanghao@mail. iggcas.ac.cn; yangyueheng@mail.iggcas.ac.cn

bInnovation Academy for Earth Science, Chinese Academy of Sciences, Beijing, 100029, P. R. China

cState Key Laboratory of Geological Processes and Mineral Resources, Institute of Earth Sciences, China University of Geosciences, Beijing, 100083, P. R. China

† Electronic supplementary information (ESI) available. See DOI: https://doi.org/10.1039/d2ja00407k

This journal is © The Royal Society of Chemistry 2023

J. Anal. At. Spectrom., 2023, 38, 1285–1300 | 1285

screening out the high Lu/Hf domains within single minerals, which is important for the success of isochron dating. The LA-ICP-MS/MS technique has been successfully applied to *in situ* Rb–Sr, K–Ca and Re–Os dating of geological samples[13–15] and has improved U–Pb dating by removing the [204]Hg interference from [204]Pb.[16,17] The *in situ* Lu–Hf dating technique with LA–ICP–MS/MS analysis was applied to Paleozoic–Precambrian garnet, apatite and xenotime samples for the first time by Simpson *et al.* (2021),[18] and then, this innovative technique has been applied to reveal unidentified multiple-stage garnet growth in subducted rocks from southern Australia.[19]

Despite the successful applications of this technology, there are several aspects for further improvement: (1) mixtures of NH_3 in He (typical NH_3 : He, 1 : 9) are commonly used as the reaction gas for separation of [176]Hf from [176]Lu and [176]Yb (*e.g.*, Simpson *et al.* 2021),[18] but He mixtures may cause the dissociation of large molecule ions and reduce the sensitivity of NH_3 reaction productions. The advantages of high-purity NH_3 and/or the optimal proportion of mixture NH_3 have not been investigated. (2) A previous study[18] documented a matrix-induced Lu–Hf bias between NIST SRM 610 and xenotime and apatite, but the benefits of using a secondary matrix matched reference material for further calibration have not been fully evaluated. (3) To date, most successful applications of *in situ* Lu–Hf dating have involved an Agilent 8900 (Agilent Technologies, USA) ICP-MS/MS system, whereas use of an iCap TQ (Thermo Fisher, USA) ICP-MS/MS system has not yet been fully explored. Here, the iCap TQ ICP-MS/MS system was optimised for *in situ* Lu–Hf geochronology. The effect of the NH_3/He ratio on the reaction efficiency of Hf with NH_3 was evaluated, together with N_2 enhancement (addition of small amounts of N_2 to the sample gas). Reaction products of Lu, Yb and Hf were identified in the mass range from 175–300 amu. Potential matrix effects on Lu/Hf ratios were evaluated and the technique was applied to xenotime, apatite and garnet samples.

2 Experimental

2.1 Sample descriptions

There is a lack of Lu–Hf age reference materials, and two categories of samples were selected for this study, including (1) reference materials for the U–Pb dating systems and (2) samples with ages constrained by well-characterized emplacement or metamorphic ages of host rocks. Ten samples were studied, five xenotime, three apatite and two garnet samples. The xenotime and apatite samples were of category (1), expect for xenotime M1567. Although several grossular- or andradite-rich garnet U–Pb reference materials (Willsboro,[20] Mali,[20] and WS20[21]) are available, they are all of igneous or metasomatic origin and have extremely low Lu/Hf ratios (<1) and thus are not suitable for Lu–Hf dating. Rather, two metamorphic garnet samples with well-characterized formation ages were used in this study. Sample details are summarised below.

2.1.1 Xenotime. Xenotime, a Y and heavy rare-earth element (HREE) orthophosphate, is a common accessory mineral for U–Th–Pb geochronology because of its high U and Th contents, low common-Pb contents, and low Pb diffusion rate (*i.e.*, a high closure temperature). Cherniak (2006)[22]

reported that the closure temperature of a U–Pb isotopic system for a grain with 10 μm effective radius is ~890 °C (for a cooling rate of 10 °C Ma^{-1}). Although the closure temperature for a Lu–Hf isotopic system in xenotime has not been well constrained, diffusion experiments showed that the activation energies for diffusion of the REE in xenotime are comparable with that for Pb diffusion (349–441 kJ mol^{-1} *vs.* 382 kJ mol^{-1}) and the tetravalent Hf would be expected to have higher activation energies for diffusion.[22] Therefore, it is reasonable to assume that Lu–Hf and U–Pb ages of xenotime are the same. In reality, the same assumption has also been made to determine the [176]Lu decay constant.[1] Sample details are summarised below.

XN02 xenotime reference materials are megacrysts collected from the Datas alluvial deposits in SE Brazil. The crystals have an average [206]Pb/[238]U age of 515.4 ± 0.2 Ma.[23] Here, the samples are used as a matrix-matched reference material to correct for matrix-induced elemental fractionation in the determination of Lu/Hf ratios in SRM 610 and xenotime.

MG-1 is a single crystal obtained from Minas Gerais, Brazil.[24] It was derived from a metamorphic rock, but its genesis is unknown. MG-1 xenotime has a [206]Pb/[238]U age of 490.0 ± 0.3 Ma with U contents of ~500 μg g^{-1} and Th/U ratios of ~3.0.

BS-1 is another single crystal obtained from Minas Gerais, with a [206]Pb/[238]U age of 508.9 ± 0.3 M, a [208]Pb/[232]Th age of 508.2 ± 0.3 Ma, U contents of ~300 μg g^{-1}, and Th/U ratios of ~8.0.[24]

XENOA is a xenotime megacryst from Brazil, but its detailed geological context is missing. Its isotope dilution (ID)-TIMS [206]Pb/[238]U and [207]Pb/[206]Pb ages are 509.9 ± 4.1 and 505.1 ± 8.0 Ma, respectively (unpublished data). This sample is used as an in house U–Pb reference material in the LA-ICP-MS laboratory at the Institute of Geology and Geophysics, Chinese Academy of Sciences (IGGCAS).

M1567 is a xenotime megacryst provided by the IGGCAS museum collected from South China, but the detailed information on sample location and host rock type is missing.

2.1.2 Apatite. Apatite (Ca$_5$(PO$_4$)$_3$(F, Cl, OH): fluorapatite, chlorapatite and hydroxylapatite, respectively) is a common accessory mineral used in U–Th–Pb geochronology in various geological settings. Apatite generally has low U contents (<50 μg g^{-1}) and variable common-Pb contents. The closure temperature of the Lu–Hf system (675–750 °C) is higher than that of the U–Pb system (350–550 °C).[25] Therefore, the apatite Lu–Hf and U–Pb ages may be decoupled and depend on the cooling rate and/or storage duration of apatite minerals.[26]

Otter Laker apatite from the Yates mine, Otter Laser area, Quebec, has been used as a U–Pb reference material (ID-TIMS [206]Pb/[238]U age of 913 ± 7 Ma) for LA-ICP-MS analysis.[27–29] There is a published Lu–Hf age (1031 ± 6 Ma) for Otter lake apatite, as well as published Lu–Hf isotopic data for cogenetic titanite, which can be used to correct Lu–Hf age data for common-Hf isotopic composition.[30] This sample contains 8–10 μg g^{-1} Lu and 0.012–0.024 μg g^{-1} Hf.

NW-1 apatite was extracted from a carbonatite from the Paririe Lake alkaline carbonatite complex, Ontario, Canada.[28] There have been many geochronological investigations conducted on this complex, and the best estimate for the [207]Pb/[206]Pb age of NW-1 apatite is 1160 ± 5 Ma.[28] This sample contains ~4.0 μg g^{-1} Lu.

1286 | *J. Anal. At. Spectrom.*, 2023, **38**, 1285–1300

This journal is © The Royal Society of Chemistry 2023

MAP-3 is an apatite megacryst used as an in house U–Pb reference material in the LA-ICP-MS laboratory at the China University of Geosciences, Beijing (CUGB). The ID-TIMS analyses yield a ^{206}Pb/^{238}U age of 800.6 ± 0.6 Ma (Duan *et al.* submitted).[31] This sample contains ∼5.0 μg g^{-1} Lu.

2.1.3 Garnet. Garnet is found in a wide range of bulk-rock compositions and is extensively used as a petrogenetic recorder of metamorphic conditions. Garnet has well-understood elemental diffusive behaviour, so it can be applied in recovering thermal histories.[32,33] Previous studies documented the LA-ICP-MS U–Pb dating technique for the ugrandite garnet that is mainly found in alkaline magmatic rocks and skarn.[20,21,34] However, pyralspite garnet, mainly found in regional metamorphic rocks, has very low U and Th contents, and thus is rarely used in U–Pb geochronology. The closure temperatures of U–Pb and Lu–Hf isotopic systems in garnet are about 750–800 °C for a grain with 100 μm effective radius at a cooling rate of 20 °C Ma^{-1}.[21,33]

14SA36 garnet is hosted by a mafic metavolcanic rock from the Barberton greenstone belt, South Africa.[35] 14SA36 garnet is compositionally homogeneous and consists mainly of almandine, grossular, and spessartine with minor pyrope. The garnet was suggested to form under the metamorphic conditions of T = 708–754 °C and P = 1.36–1.45 Ga. The zircons that were equilibrated with garnet during metamorphism gave a weighted mean ^{207}Pb/^{206}Pb age of 3226.3 ± 5.5 Ma.[35] Given the high closure temperature of the Lu–Hf isotopic system in garnet, we inferred that 14SA36 garnet has a Lu–Hf age of *ca.* 3226 Ma.

12QL59 garnet is from a felsic gneiss that was sampled from the Songshugou area, North Qinling orogen. The gneiss is composed mainly of garnet, amphibole, biotite, plagioclase, perthite and quartz, and was suggested to record a metamorphic temperature of >850 °C. The garnet is predominated by almandine and pyrope with minor grossular and spessartine. The metamorphic zircons in this sample defined a weighted mean ^{206}Pb/^{238}U age of 489 ± 4 Ma (unpublished data), which is adopted as the Lu–Hf age of the garnet considering the high closure temperature of the Lu–Hf system.

2.2 Instrumentation

In situ Lu–Hf dating analyses involved a Photon Machines Analyst G2 laser ablation system (Teledyne CETAC, Omaha, USA) coupled to an iCap TQ ICP-MS/MS (Thermo Fisher Scientific, Bremen, Germany). ICP-MS/MS conditions were first optimised in the solution single-quadrupole (SQ) and no-gas modes (*i.e.*, with no NH$_3$ in the reaction cell) to tune the system for a robust plasma (U/Th = 1.00–1.05) and to minimise oxide interferences (ThO/Th < 0.5%); Then, the instrument was switched to triple-quadrupole (TQ) and NH$_3$ mode. The lenses were tuned to maximise sensitivity for Hf reaction products while maintaining relatively low Lu and Yb reaction rates. A small amount of N$_2$ (4.0 mL min^{-1}) was added to the carrier gas after the sample chamber to enhance sensitivity.[36,37] LA-ICP-MS/MS tuning and analysis parameters are summarised in Table 1. High-purity (>99.999%) NH$_3$ was used as the reaction gas, supplied in T4 (Tube 4). High-purity (>99.999%) He (supplied in T1) was pre-mixed with NH$_3$ before the reaction cell to test the effect of mixture composition on reaction efficiency.

Laser spot diameters were set to 50–150 μm (Table 1), depending on the Lu and Hf contents. The isotopes analysed were those necessary for Lu–Hf geochronology, plus a selection of elements for monitoring inclusions such as Zr for zircons. The isotopes and ammonia cluster ions analysed were ^{27}Al, ^{43}Ca, ^{89}Y, ^{90}Zr, ^{172}Yb, $^{(172+82)}$Yb (expressed for ^{172}Yb(^{14}N^{1}H)(^{14}N^{1}H$_2$) (^{14}N^{1}H$_3$)$_3$, mass shift by +82), ^{175}Lu, $^{(175+82)}$Lu (^{175}Lu(^{14}N^{1}H)(^{14}N^{1}H$_2$) (^{14}N^{1}H$_3$)$_3$), $^{(176+82)}$Hf (^{176}Hf(^{14}N^{1}H)(^{14}N^{1}H$_2$) (^{14}N^{1}H$_3$)$_3$), $^{(177+82)}$Hf (^{177}Hf(^{14}N^{1}H)(^{14}N^{1}H$_2$) (^{14}N^{1}H$_3$)$_3$)and $^{(178+82)}$Hf(^{178}Hf(^{14}N^{1}H)(^{14}N^{1}H$_2$) (^{14}N^{1}H$_3$)$_3$). The numbers (M_1 + M_2) in brackets represent the original mass number of isotopes (M_1) plus the mass shift number by using the ammonia cluster (M_2). Owing to their higher abundance and a lack of isobaric interferences, ^{175}Lu was monitored as a proxy for ^{176}Lu and ^{178}Hf as a proxy for ^{177}Hf. As these are stable isotopes, the present day ^{176}Lu/^{175}Lu and ^{177}Hf/^{178}Hf ratios of 0.02655 and 0.682 (ref. 38) were used to calculate ^{176}Lu and ^{177}Hf contents.

Simpson *et al.*[18] documented a potential isobaric interference for $^{(176+82)}$Hf from residual $^{(175+83)}$Lu (^{175}Lu(^{14}N^{1}H)(^{14}N^{1}H$_3$)$_4$$^+$) ions (258 amu, equivalent to $^{(176+82)}$Hf) not fully extracted from the collision/reaction cell after switching Q1 from mass 175 to 176 amu, and they proposed a 5 ms wait time offset (WTO) to allow Lu cluster ions to exit the cell before measurement of $^{(176+82)}$Hf. Such a specific WTO could not be set for the iCap TQ instrument, so in this study, a short dwell time (1 ms) for ^{175}Lu was used to reduce this potential interference by largely decreasing the entered amount of ^{175}Lu ions. Xenotime analyses indicated that this approach eliminated the $^{(175+83)}$Lu interference effectively from $^{(176+82)}$Hf (Table 2).

2.3 Data processing

Lu–Hf data were processed using the Iolite v.3.7 software package.[39] Raw data (time-resolved intensities) from the mass spectrometer were loaded into Iolite v.3.7 to calculate gas-blank-corrected intensities, raw ratios (*e.g.*, ^{176}Lu/^{177}Hf and ^{176}Hf/^{177}Hf) and their uncertainties. Other corrections of instrument drift, elemental fractionation and matrix induced bias were made using an in-house Microsoft Excel spreadsheet. The potential interferences of ^{176}Lu and ^{176}Yb on ^{176}Hf were monitored by measuring ^{175}Lu and ^{172}Yb archives, and corrected as follows:

$$^{(176+82)}\text{Hf}_{\text{measured}} = {}^{(176+82)}\text{total} - \left(\frac{^{(176)}\text{Lu}}{^{(175)}\text{Lu}}\right)_{\text{true}} \times {}^{(175+82)}\text{Lu}_{\text{measured}}$$
$$- \left(\frac{^{(176)}\text{Yb}}{^{(172)}\text{Yb}}\right)_{\text{true}} \times {}^{(172+82)}\text{Yb}_{\text{measured}}$$

$$(1)$$

$$p_{\text{Lu}}(\%) = \frac{\left(\frac{^{(176)}\text{Lu}}{^{(175)}\text{Lu}}\right)_{\text{true}} \times {}^{(175+82)}\text{Lu}_{\text{measured}}}{^{(176+82)}\text{total}} \times 100 \quad (2)$$

This journal is © The Royal Society of Chemistry 2023

J. Anal. At. Spectrom., 2023, **38**, 1285–1300 | **1287**

Table 1 LA-ICP-MS/MS tuning and analysis parameters

Laser ablation system

Make, model & type	Photon Machines Analyte G2
Ablation cell	HelEx ablation cell
Laser wavelength	193 nm
Pulse width	4–5 ns
Energy density/fluence	4 J cm^{-2}
Repetition rate	10 Hz
Spot size	50, 90, 150 μm
Sampling mode/pattern	Single hole drilling, two cleaning pulses
Ablation gas flow (He)	900 mL min^{-1}
Ablation duration	25 s

ICP-MS/MS

Make, model & type	Thermal iCap TQ
RF power	1350 W
Sample cone	High sensitivity
Skimmer cone	High sensitivity
Coolant gas flow (Ar)	15.00 L min^{-1}
Auxiliary gas flow (Ar)	0.80 L min^{-1}
Carrier gas flow (Ar)	0.65 L min^{-1}
Enhancement gas flow (N$_2$)	4.0 mL min^{-1}
Scan mode	Peak jump
Isotopes measured (*m/z*) + sample time	^{27}Al (2 ms), ^{43}Ca (2 ms), ^{89}Y (1 ms), ^{90}Zr (2 ms), ^{172}Yb (1 ms), $^{(172+82)}$Yb (100 ms), ^{175}Lu (1 ms), $^{(175+82)}$Lu (50 ms), $^{(176+82)}$Hf (300 ms), $^{(177+82)}$Hf (100 ms) and $^{(178+82)}$Hf (100 ms)
Detection system	Single SEM in double mode, counting and analog
Resolution	~300
Total integration time per reading	0.659 s

Lens parameters
Major

Extraction lens 2 (V)	−130.0
Angular deflection (V)	−250.0
Q1 entry lens(V)	−94.50
Q1 focus lens(V)	0.100
Focus lens(V)	1.000
Q1 pole bias (V)	0.000
CR bias (V)	−4.200
Q3 pole bias	−12.00

Minor

Extraction len 1 positive (V)	0.000
Deflection entry lens (V)	−30.00
CR entry lens (V)	−144.0
CR amplitude (V)	189.3
CR exit lens (V)	−40.00
D1 lens (V)	−350.0
D2 lens (V)	−159.4
Q3 entry lens (V)	−56.00

$$p_{\mathrm{Yb}}(\%) = \frac{\left(\frac{^{(176)}\mathrm{Yb}}{^{(172)}\mathrm{Yb}}\right)_{\mathrm{true}} \times {}^{(172+82)}\mathrm{Yb}_{\mathrm{measured}}}{^{(176+82)}\mathrm{total}} \times 100 \qquad (3)$$

where $^{(176+82)}$total is the total signal intensity at (176 + 82) mass; $^{(176+82)}$Hf$_{\mathrm{measured}}$ is the measured signal intensity of $^{(176+82)}$Hf; $^{(175+82)}$Lu$_{\mathrm{measured}}$ is the signal intensity of $^{(175+82)}$Lu; $^{(172+82)}$Yb$_{\mathrm{measured}}$ is the signal intensity at $^{(172+82)}$Yb; the used $\left(\frac{^{(176)}\mathrm{Lu}}{^{(175)}\mathrm{Lu}}\right)_{\mathrm{true}}$ and $\left(\frac{^{(176)}\mathrm{Yb}}{^{(172)}\mathrm{Yb}}\right)_{\mathrm{true}}$ ratios are 0.02655 and 0.5887, respectively; and p_{Lu} (%) and p_{Yb} (%) are the contributions of isobaric interferences on $^{(176+82)}$Hf signal intensities.

The mass bias of $\left(\frac{^{(176)}\mathrm{Lu}}{^{(177+82)}\mathrm{Hf}}\right)$ and isotope fractionation of $\left(\frac{^{(176+82)}\mathrm{Hf}}{^{(177+82)}\mathrm{Hf}}\right)$ were externally corrected by analysis of NIST SRM 610 using the recommended values of 0.1379 ± 0.0050 and 0.282111 ± 0.000009, respectively, as determined by ID-MC-ICP-MS.[40] Due to the higher isotopic abundance of ^{178}Hf (27.297%) than ^{177}Hf (18.606%), the $^{(178+82)}$Hf was monitored as a proxy for $^{(177+82)}$Hf, and its signal intensity was calculated from $^{(178+82)}$Hf using a $\left(\frac{^{(177)}\mathrm{Hf}}{^{(178)}\mathrm{Hf}}\right)$ ratio of 0.682. The ^{176}Lu signal intensity was

Table 2 Summary of LA-ICP-MS/MS data of xenotime, apatite and garnet[a]

Sample name	Numbers (n)	Signal intensity (cps)					Contributions			Reaction rate (%)		Ratios		Concentrations (µg g⁻¹)		Single spot Lu–Hf ages		
		^{172}Yb	^{175}Lu	^{176}Hf	^{177}Hf	^{178}Hf	p_{Lu} (%)	p_{Yb} (%)	$f_{^{174}\text{Hf}}$	Lu	Yb	^{172}Yb/^{177}Hf	^{175}Lu/^{177}Hf	Yb/Lu	Lu	Age (Ma)	Uncertainty (2s, Ma)	Uncertainty* (2s, Ma)
XN02	246	2.57×10^7	1.12×10^7	1690	386	559	0.6	3.0	7.1	0.00347	0.00033	14 681	11 400	8.32	5124	515.4	1.2	7.4
MG-1	163	5.76×10^6	1.76×10^6	264	48.0	68.0	0.7	4.9	6.3	0.00380	0.00039	24 665	13 825	11.5	839	489.2	2.1	7.2
BS-1	33	1.58×10^7	6.34×10^6	483	103	150	1.6	3.5	6.4	0.00441	0.00018	22 738	15 410	9.63	3654	509.4	4.7	8.6
XenoA	25	1.24×10^7	4.32×10^6	365	21.2	27.2	1.8	3.9	1.5	0.00598	0.00020	100 899	57 446	11.6	2091	508.6	7.5	10.4
M1567	34	3.32×10^7	1.86×10^7	1160	2260	3350	2.3	2.3	59.0	0.00631	0.00018	1649	1598	6.87	4397	181.6	2.1	3.3
Otter lake	20	2.68×10^5	1.37×10^5	23.3	7.60	11.9	1.0	0.0	9.3	0.00620	0.00032	5346	4290	8.17	9.37	1038	32	35
NW-1	20	1.20×10^5	5.20×10^4	13.8	22.1	30.7	0.3	0.0	43.7	0.00400	0.00044	782	543	9.70	4.21	1147	87	88
MAP-3	38	9.25×10^4	5.37×10^4	10.3	0.43	0.87	0.0	0.0	1.4	0.00510	0.00026	21 579	22 288	6.55	5.67	865	25	27
14SA36	73	3.99×10^4	2.39×10^4	105	248	346	0.0	0.0	79.2	—	—	34.0	41.0	6.09	0.71	3244	33	57
12QL59	38	9.96×10^4	4.95×10^4	17.2	34.0	48.3	0.0	0.0	61.2	—	—	687	611	7.26	2.33	486.0	12.9	39.9

[a] The values of signal sensitivity (cps), interference contribution (p_{Lu} and p_{Yb}), reaction rate (%), isotope ratio and concentration (µg g⁻¹) are given in the median of the dataset. $f_{^{174}\text{Hf}}$ (%) is the fraction of common Hf. A value of 0.282 ± 0.004 was used to cover all likely crustal ^{176}Hf/^{177}Hf ratios for the generation of common-Hf corrected single-spot ages, except for the garnet samples (the common-Hf corrected single-spot ages were calculated using isochron intercepts as the ^{176}Hf/^{177}Hf-ratios). The uncertainty marked with "*" represents the one after the propagation of initial ^{176}Hf/^{177}Hf uncertainty (for xenotime and apatite, 0.004 of 0.282 is propagated; for garnet, the uncertainty of intercept ^{176}Hf/^{177}Hf is used).

calculated from ^{175}Lu using a $\left(\frac{^{(176)}\text{Lu}}{^{(175)}\text{Lu}}\right)$ ratio of 0.02655. The following equations were applied:

$$\left(\frac{^{(176)}\text{Lu}}{^{(177+82)}\text{Hf}}\right)_{\text{corrected, sample}} = \left(\frac{^{(176)}\text{Lu}}{^{(177+82)}\text{Hf}}\right)_{\text{measured, sample}}$$
$$\times \left(\frac{^{(176)}\text{Lu}}{^{(177)}\text{Hf}}\right)_{\text{true, NIST 610}}$$
$$\div \left(\frac{^{(176)}\text{Lu}}{^{(177+82)}\text{Hf}}\right)_{\text{measured, NIST 610}}$$

(4)

$$\left(\frac{^{(176+82)}\text{Hf}}{^{(177+82)}\text{Hf}}\right)_{\text{corrected, sample}} = \left(\frac{^{(176+82)}\text{Hf}}{^{(177+82)}\text{Hf}}\right)_{\text{measured, sample}}$$
$$\times \left(\frac{^{(176)}\text{Hf}}{^{(177)}\text{Hf}}\right)_{\text{ture, NIST610}} \div \left(\frac{^{(176+82)}\text{Hf}}{^{(177+82)}\text{Hf}}\right)_{\text{measured, NIST 610}}$$

(5)

where $\left(\frac{^{(176)}\text{Lu}}{^{(177+82)}\text{Hf}}\right)_{\text{measured}}$ and $\left(\frac{^{(176+82)}\text{Hf}}{^{(177+82)}\text{Hf}}\right)_{\text{measured}}$ are the measured isotopic ratios and $\left(\frac{^{(176)}\text{Lu}}{^{(177+82)}\text{Hf}}\right)_{\text{corrected}}$ and $\left(\frac{^{(176+82)}\text{Hf}}{^{(177+82)}\text{Hf}}\right)_{\text{corrected}}$ are the corrected isotopic ratios.

A matrix-induced mass bias of $\left(\frac{^{(176)}\text{Lu}}{^{(177+82)}\text{Hf}}\right)$ ratios between SRM 610 and the samples was observed, so further correction was necessary using a matrix-matched sample (e.g., XN02 for xenotime samples). This matrix-induced mass bias varied among different analytical sessions, as discussed in Section 3.

The radiogenic ^{176}Hf content was corrected from the common-Hf component for the single-spot age calculations, as follows:

$$^{(177+82)}\text{Hf}_{\text{common}} = \left(\frac{^{(176)}\text{Hf}}{^{(177)}\text{Hf}}\right)_{\text{initial}} \times {}^{(176+82)}\text{Hf}_{\text{measured}}$$

(6)

$$^{(176+82)}\text{Hf}_{\text{radiogenic}} = {}^{(176+82)}\text{Hf}_{\text{measured}} - {}^{(176+82)}\text{Hf}_{\text{common}}$$

(7)

$$f_{(176)\text{Hf}}(\%) = \frac{^{(176+82)}\text{Hf}_{\text{common}}}{^{(176+82)}\text{Hf}_{\text{measured}}} \times 100$$

(8)

where $^{(176+82)}\text{Hf}_{\text{radiogenic}}$ is radiogenic $^{(176+82)}\text{Hf}$, $^{(176+82)}\text{Hf}_{\text{common}}$ is the common $^{(176+82)}\text{Hf}$ and $^{(177+82)}\text{Hf}_{\text{measured}}$ is the measured $^{(177+82)}\text{Hf}$. As $\left(\frac{^{(176)}\text{Hf}}{^{(177)}\text{Hf}}\right)_{\text{initial}}$ ratios are relatively uniform over Earth's history, a value of 0.282 ± 0.004 (1.4%) could cover all likely crustal ^{176}Hf/^{177}Hf ratios and was used to calculate single-spot ages when isochron intercept ^{176}Hf/^{177}Hf ratios were not obtained. The same initial Hf ratio has been used in the previous study.[18] $f_{(176)\text{Hf}}$ (%) is the fraction of common Hf.

The isochron age equation[5] is,

$$\left(\frac{^{(176+82)}\text{Hf}_{\text{measured}}}{^{(177+82)}\text{Hf}}\right)_{\text{corrected}} = \left(\frac{^{(176)}\text{Hf}}{^{(177)}\text{Hf}}\right)_{\text{initial}} + \left(\frac{^{(176)}\text{Lu}}{^{(177+82)}\text{Hf}}\right)_{\text{corrected}}$$
$$\times \left(e^{\lambda t} - 1\right)$$

(9)

where λ is the decay constant of ^{176}Lu. This equation can be rearranged as follows:

This journal is © The Royal Society of Chemistry 2023

J. Anal. At. Spectrom., 2023, **38**, 1285–1300 | 1289

$$\left(\frac{^{(176+82)}\text{Hf}_{\text{radiogenic}}}{^{(177+82)}\text{Hf}}\right)_{\text{corrected}} = \left(\frac{^{(176+82)}\text{Hf}_{\text{measured}}}{^{(177+82)}\text{Hf}}\right)_{\text{corrected}}$$
$$- \left(\frac{^{(176)}\text{Hf}}{^{(177)}\text{Hf}}\right)_{\text{initial}}$$
$$= \left(\frac{^{(176)}\text{Lu}}{^{(177+82)}\text{Hf}}\right)_{\text{corrected}} \times \left(e^{\lambda t} - 1\right)$$

$$(10)$$

which can be simplified and rearranged to solve for time:

$$t = \frac{\text{Ln}\left\{1 + \left(\dfrac{^{(176+82)}\text{Hf}_{\text{radiogenic}}}{^{(176)}\text{Lu}}\right)_{\text{corrected}}\right\}}{\lambda}$$

$$(11)$$

Single-spot ages were calculated using eqn (11). The $\left(\frac{^{(176)}\text{Lu}}{^{(177+82)}\text{Hf}}\right)_{\text{corrected, sample}}$ and $\left(\frac{^{(176+82)}\text{Hf}}{^{(177+82)}\text{Hf}}\right)_{\text{corrected, sample}}$ ratios and their uncertainties were used to construct isochron ages. Isoplot R software was used to calculate isochron and weighted-mean ages.[41] The uncertainty propagation workflow reported by Rösel and Zack[42] was adopted in this study. The final uncertainties incorporate both the random uncertainties (*e.g.*, measured ratios) and systematic uncertainties (*e.g.*, uncertainties of the reference material, long-term variance, uncertainty of the decay constant and uncertainty of initial $^{176}\text{Hf}/^{177}\text{Hf}$). The long-term variance was set to be 1.5% and the uncertainty of initial $^{176}\text{Hf}/^{177}\text{Hf}$ is 1.4% (0.004 of 0.282).

Lutetium and Hf concentrations were calculated using Iolite software with "Trace_Element" DRS and the semi quantitative standardisation method of Paton *et al.*[39] NIST SRM 610 was used for external calibration and ARM-1 (ref. 43 and 44) is used for the quality control. The results were consistent with published data within ±20% of relative discrepancy.

3 Results and discussion

3.1 Signal sensitivity in different analytical modes

The iCap TQ ICP-MS/MS was used in either SQ or TQ mode. In TQ mode, the first quadrupole (the prefiltered quadrupole) can be run in two ways: 'normal', with a mass resolution of 10 amu; and 'high', with a mass resolution of 1 amu. To avoid interference from ^{175}Lu reaction products during *in situ* Lu–Hf dating analysis, the required prefiltered mass resolution is 1 amu.[18] We compared the sensitivity of ^{178}Hf in five different modes (Fig. 1). Data were collected in LA mode. Signal intensities were monitored by ablating SRM 610 with 20 μm spot size, 10 Hz frequency, 1 μm s^{-1} line scanning speed and ~3.0 J cm^{-2} energy density. As shown in Fig. 1, the SQ analytical mode provides the highest sensitivity. The usage of Q1 will inevitably reduce the sensitivity owing to its 'filtration' effect, which was strongest with Q1 at high resolution (1 amu).

Sensitivity in the 'CR (collision and reaction) gas: NH$_3$ = 0' mode was lower than that in the 'CR gas: none' mode, which is likely related to the automatically set voltage parameters of the instrument. The sensitivity to reaction products of $^{(180+82)}\text{Hf}$ (expressed for ^{180}Hf $(^{14}\text{N}^1\text{H})(^{14}\text{N}^1\text{H}_2)$ $(^{14}\text{N}^1\text{H}_3)_3{}^+$, mass shift by +82) in TQ mode with 'CR gas: NH$_3$ = 0.325 mL min^{-1}' accounted for ~60% of the sensitivity for ^{180}Hf in the TQ mode with 'CR gas: NH$_3$ = 0 mL min^{-1}'. The low abundance of ^{176}Hf requires a more sensitive instrument for *in situ* Lu–Hf dating. Previous studies have found that a small amount of N$_2$ added to the sample gas flow improved the sensitivity of Agilent 7500/ 7900 and Thermo Element XR instruments.[36,37] We tested this using the Thermo iCap TQ ICP-MS/MS system and found an 80% increase in sensitivity with an N$_2$ flow rate of 4.0 mL min^{-1} (Fig. 1).

3.2 Identification of reaction products

Reaction products of Hf with NH$_3$ have been investigated using an Agilent 8900 ICP-MS/MS instrument,[12,18] but this does not seem to have previously been considered using the iCap TQ ICP–MS/MS instrument. Here, the reaction products of Hf, Yb and Lu were identified in the mass range of 175–300 amu (Fig. 2). The abundance of ^{15}N (0.366%) and ^2H (0.015%) is much less than those of ^{14}N (99.634%) and ^1H (99.985%); therefore, the reaction products involving ^{15}N and ^2H were ignored in the mass spectrum. Data were collected in solution mode with injection of 0.1 μg g^{-1} Yb, Lu and Hf single standard solutions. In the Lu reaction experiment, a mass-176 filter was initially used in Q1, but an interference of $^{175}\text{Lu}^1\text{H}^+$ on $^{176}\text{Lu}^+$ was observed. Therefore, a mass-175 filter was used, and the reaction products of Lu were monitored by $^{175}\text{Lu}^+$. For better comparison, the mass spectrogram of Lu was scaled to $^{176}\text{Lu}^+$ from $^{175}\text{Lu}^+$ by using the mass shift and isotopic abundance. As shown in Fig. 2, reaction products and reaction efficiencies of Hf, Lu and Yb were different. The reaction efficiency for Hf was much higher than those for Yb and Lu, with >98.5% of ^{176}Hf reacted to NH products and only 16.7% and 0.3% for ^{176}Lu and ^{176}Yb, respectively.

Major reaction products of Yb, Lu and Hf are marked in Fig. 2. There are 14, 7 and 2 main reaction products for Hf, Lu
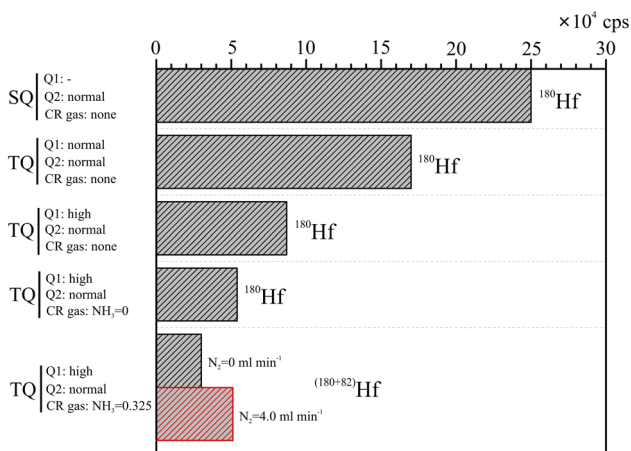

Fig. 1 Signal intensity of ^{180}Hf with different instrument modes. SQ, single quadrupole; TQ, triple quadrupole. Data were obtained by line scanning ablation of NIST SRM 610 with 20 μm spot size, 1.0 μm s^{-1} scanning speed rate, 10 Hz frequency and ~3.0 J cm^{-2} energy density. The SQ mode provided greatest sensitivity. A small amount of N$_2$ improved signal sensitivity by ~80%.

1290 | *J. Anal. At. Spectrom.*, 2023, **38**, 1285–1300

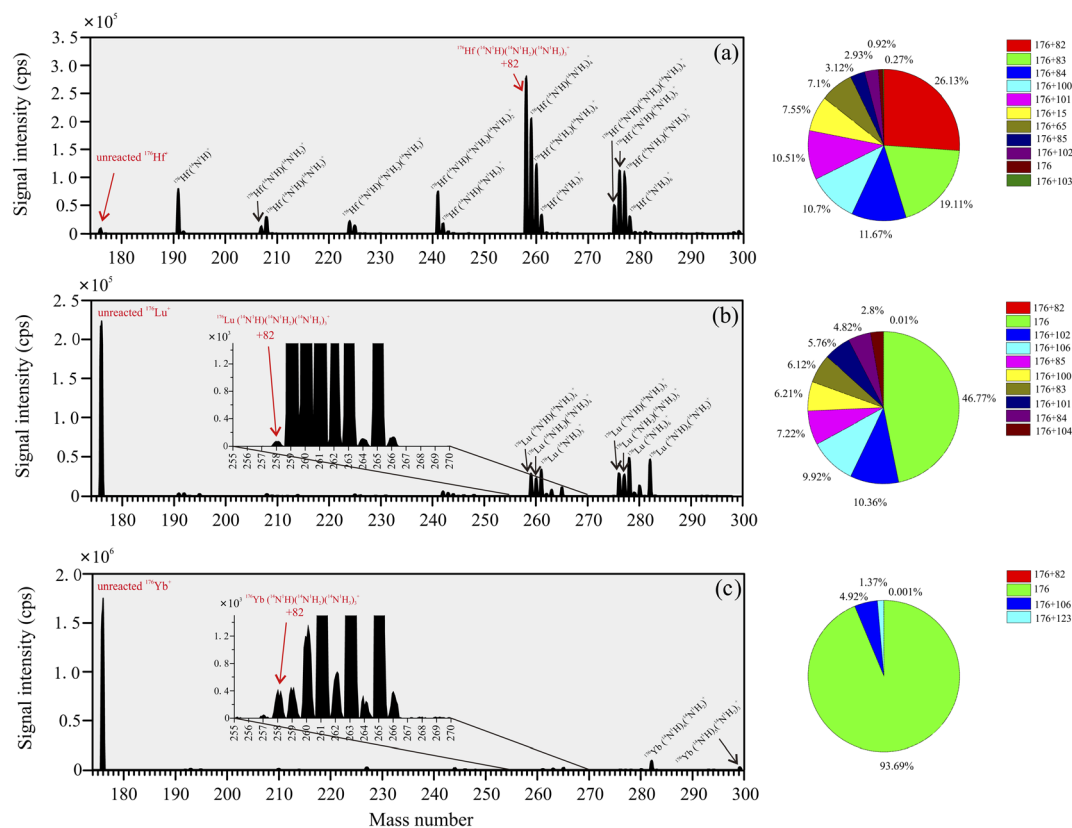This journal is © The Royal Society of Chemistry 2023

Fig. 2 The reaction products of Hf (a), Lu (b) and Yb (c) in the mass range of 175–300 amu. The abundance of ^{15}N (0.366%) and ^{2}H (0.015%) is much less than those of ^{14}N (99.634%) and ^{1}H (99.985%); therefore, the reaction products involving ^{15}N and ^{2}H were ignored in the mass spectrum. Data were collected in solution mode with injection of 0.1 µg g^{-1} Yb, Lu and Hf single-standard solution. $^{176}Hf^{+}$ and $^{176}Yb^{+}$ were used for the Hf and Yb experiment, and $^{175}Lu^{+}$ was used for the Lu experiment. For a better comparison, the mass spectrogram of Lu was scaled to $^{176}Lu^{+}$ from $^{175}Lu^{+}$ by using the mass shift and isotopic abundance. Hf is more effective with NH_3 compared with Lu and Yb. Proportions (%) of major reaction products are shown in the pie charts.

and Yb, respectively. The highest-reaction-rate products were +82 for ^{176}Hf, +102 for ^{176}Lu, and +106 for ^{176}Yb, respectively. Lutetium has a strong tendency to react with one more H than Hf at more complex adduct ions,[12,18] minimising mass interferences for ^{176}Hf; this also occurred in the iCap TQ ICP-MS/MS system (Fig. 2). The proportions (%) of the most 14, 7 and 2 reaction products of Hf, Lu and Yb were calculated as shown in Fig. 2. The reaction proportions (%) were calculated from individual signal intensities without considering the sensitivities of different reaction products. The ideal reaction product for separation of ^{176}Hf from ^{176}Lu and ^{176}Yb has a mass of 258, and there was a weak signal at mass-258 for ^{176}Lu and ^{176}Yb (Fig. 2). This was also reported for the Agilent 8900 ICP-MS/MS system studied by Woods[12] and Simpson.[18] Therefore, it seems that the reaction products of Hf, Lu and Yb with NH_3 reaction gas are similar and independent of instrumentation. Both Agilent 8900 and Thermo iCap TQ instruments can properly resolve the ^{176}Hf from ^{176}Yb and ^{176}Lu isobars with the introduction of NH_3 reaction gas.

3.3 Optimization of the NH_3 flow rate

Previous studies have used a 1/9 NH_3/He mixture as the reaction gas owing to the corrosivity and difficulty of preservation and
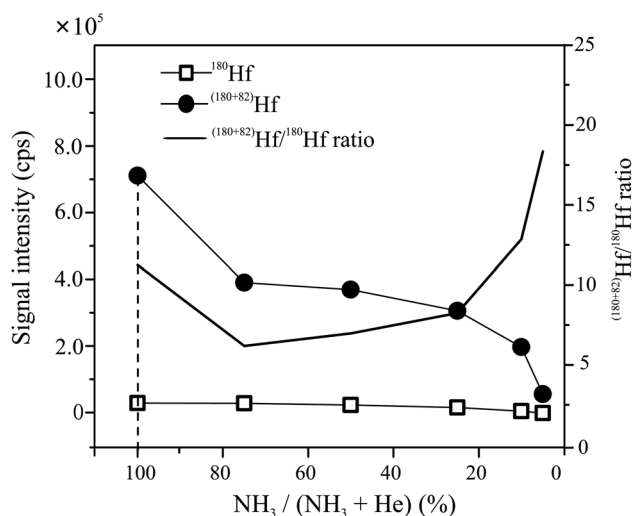

Fig. 3 Signal sensitivity of ^{180}Hf and $^{(180+82)}Hf$ with different NH_3/He ratios achieved by changing the He flow rate with a constant NH_3 flow rate of 0.325 mL min^{-1}. Data were obtained by line scanning ablation of SRM 610 with 60 µm spot size, 1.0 µm s^{-1} scanning speed rate, 10 Hz frequency and 4.0 J cm^{-2} energy density.
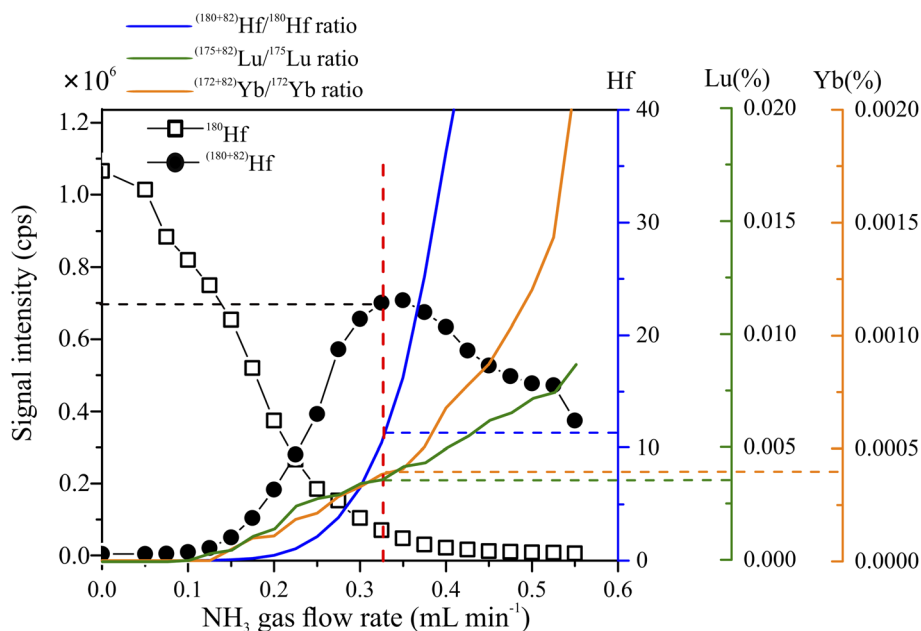
Fig. 4 Signal sensitivity for ^{180}Hf and $^{(180+82)}$Hf with different NH$_3$ gas flow rates. Ratios of $^{(180+82)}$Hf to ^{180}Hf, $^{(172+82)}$Yb to ^{172}Yb and $^{(175+82)}$Lu to ^{175}Lu are plotted as shown by colour. Owing to their low reaction efficiency, Yb and Lu are given in % values. Data were obtained by line scanning ablation of SRM 610 with 60 μm spot size, 1 μm s^{-1} scanning speed rate, 10 Hz frequency and 4.0 J cm^{-2} energy density. The optimal NH$_3$ gas flow rate was 0.325 mL min^{-1}.

transportation of high-purity NH$_3$.[16,18] The tube systems of the iCap TQ ICP-MS/MS system are specifically designed for high-purity NH$_3$ with the capability of online pre-mixing of different gases (*e.g.*, with different NH$_3$/He ratios). The gas flow pressures of NH$_3$ and He were well-controlled at the same value (~0.15 MPa) by using pressure gauges, and the mass flowmeter precisely controls the amount of NH$_3$ and He flowing into the CR cell. Pure NH$_3$ was found to be more efficient to react with Hf than NH$_3$/He mixtures (Fig. 3), which was expected, as the introduction of He gas increases the collision probability and decreases the energy of large molecule ions, and therefore reduces the sensitivity to higher-mass reaction products.

^{180}Hf has the highest abundance among the six Hf isotopes. Therefore, the signal intensities of ^{180}Hf and $^{(180+82)}$Hf (expressed for ^{180}Hf (^{14}N^{1}H)(^{14}N^{1}H$_2$) (^{14}N^{1}H$_3$)$_3$, mass shift by +82) are chosen to be shown in Fig. 4 as a function of NH$_3$ flow rate for data collected by line-scanning ablation of NIST SRM 610 with a 60 μm spot size, 10 Hz frequency and 1 μm s^{-1} scanning speed. Ratios of $^{(180+82)}$Hf to ^{180}Hf are plotted together with the signal intensities. To evaluate the potential interference from ^{176}Lu and ^{176}Yb reaction products, non-interference $^{(175+82)}$Lu to ^{175}Lu and $^{(172+82)}$Yb to ^{172}Yb ratios were plotted as functions of NH$_3$ flow rates (Fig. 4). ^{180}Hf intensities decreased with increasing NH$_3$ flow rate, whereas $^{(180+82)}$Hf intensities increased to a peak and then decreased. The increase in $^{(180+82)}$Hf intensity was likely due to incremental reaction products; after the peak, the decrease in $^{(180+82)}$Hf intensity was due mainly to the collisions between reaction products and NH$_3$ ions. The optimal NH$_3$ gas flow rate was 0.325 mL min^{-1} with a $^{(180+82)}$Hf/^{180}Hf ratio of ~10. The $^{(175+82)}$Lu/^{175}Lu and

$^{(172+82)}$Yb/^{172}Yb ratios were ~0.004% and ~0.0004%, respectively.

The long-term reaction rates (reacted/unreacted fractions) of Lu and Yb were obtained by monitoring ^{175}Lu, $^{(175+82)}$Lu, ^{172}Yb and $^{(172+82)}$Yb contents for XN02 xenotime in six sessions over three months (Fig. 5). The reaction rate of Lu ranged from 0.0027% to 0.0045% (mean 0.0034%), and those of Yb ranged from 0.00025% to 0.00048% (mean 0.00036%). Reaction rates for Lu obtained using the iCap TQ ICP-MS were similar to those
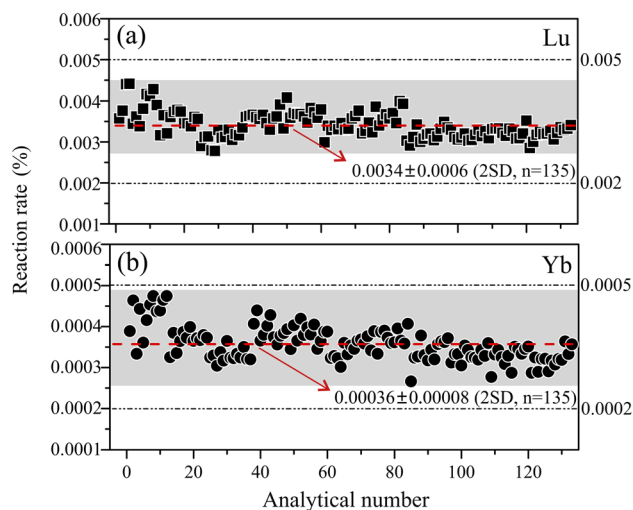

Fig. 5 Plots illustrating reaction rates of (a) Lu ($^{(175+82)}$Lu to ^{175}Lu) and (b) Yb ($^{(172+82)}$Yb to ^{172}Yb) in 10 independent analytical sessions over 3 months. The material used for these data is XN02. The reaction rates of Lu and Yb were ~0.0034% and ~0.00036%, respectively.

of the Agilent 8900 ICP-MS/MS (~0.003%; Simpson *et al.* 2021 (ref. 18)), whereas the reaction rates for Yb (~0.00036%) were an order of magnitude higher than those of the Agilent 8900 ICP-MS/MS system (~0.00003%).[18]

3.4 Separation of [176]Hf from [176]Lu and [176]Yb and potential corrections

A modelling experiment was undertaken to further evaluate the separation of [176]Hf from [176]Lu and [176]Yb in *in situ* Lu–Hf

analyses. Biases of [176]Hf/[177]Hf ratios with changing [175]Lu/[177]Hf and [172]Yb/[177]Hf ratios for different reaction rates of Lu and Yb (0.005% and 0.002% for Lu; 0.0005% and 0.0002% for Yb) are plotted in Fig. 6 (a–d). Biases in [176]Hf/[177]Hf ratios were calculated using the expression ([176]Total/[177]Hf–[176]Hf/[177]Hf)/[176]Hf/[177]Hf*100. Dark grey zones (Fig. 6) represent the analytical precision (2%) for [176]Hf/[177]Hf ratios. [175]Lu/[177]Hf and [172]Yb/[177]Hf data for xenotime, apatite and garnet samples were plotted. Xenotime samples included BS-1,
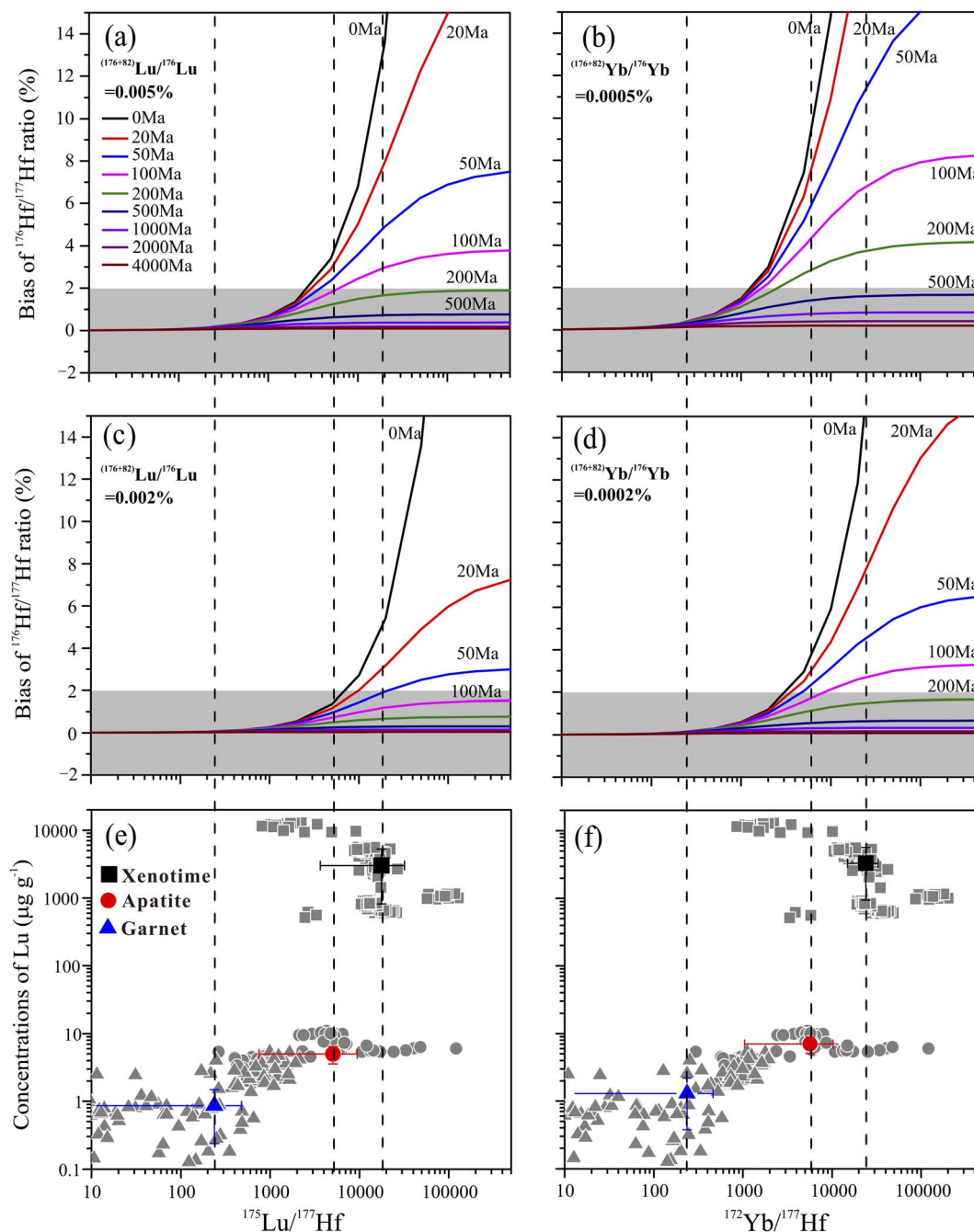
Fig. 6 Plots illustrating the bias in [176]Hf/[177]Hf ratios with different [175]Lu/[177]Hf and [172]Yb/[177]Hf ratios at ages of 0, 20, 50, 100, 200, 500, 1000, 2000 and 4000 Ma (a–d). [175]Lu/[177]Hf and [172]Yb/[177]Hf ratios and Lu (e and f) contents of xenotime, apatite and garnet are plotted to indicate potential corrections. To avoid the effect of anomalous data, median values were calculated and plotted here. Xenotime samples included BS-1, MG-1, XN02, XENOA and M1567; apatite samples included Otter Lake, NW-1 and MAP-3; and garnet samples included 14SA36 and 12QL59.

This journal is © The Royal Society of Chemistry 2023

J. Anal. At. Spectrom., 2023, **38**, 1285–1300 | **1293**

MG-1, XN02, XENOA and M1567; apatite samples were Otter Lake, NM-1 and MP3; garnet samples were 14SA36 and 12QL59. In general, the older the age, the more radioactive the accumulation of ^{176}Hf, and therefore, the lower the effect of ^{176}Lu and ^{176}Yb interferences on ^{176}Hf.

Xenotime has high contents of Lu and high values of ^{175}Lu/^{177}Hf (median ~13 000) and ^{172}Yb/^{177}Hf (median ~21 000) ratios (Fig. 6e and f). Based on reaction rates of ~0.005% and ~0.0005% for Lu and Yb, respectively, for the >500 Ma xenotime samples, there is no need for correction of ^{176}Lu and ^{176}Yb interferences on ^{176}Hf. For the >300 Ma apatite samples, with reaction rates of ~0.005% and ~0.0005% for Lu and Yb, respectively, there is no need for correction. For the garnet samples with low values of ^{175}Lu/^{177}Hf (median ~190) and ^{172}Yb/^{177}Hf (median ~190) ratios, there is no need for correction, even for samples of young to moderate age. Xenotime samples have high contents of Lu (median ~2900 μg g^{-1}), whereas apatite and garnet samples have relatively low contents of Lu (medians of ~6.0 μg g^{-1} and ~1.0 μg g^{-1}, respectively).

3.5 Matrix effects on the Lu/Hf ratio and calibration procedures

Owing to the physical and chemical properties of target minerals, matrix-induced element fractionation always occurs during LA-ICP-MS analyses, leading to systematic offsets between expected and measured ratios.[45] Simpson *et al.*[18] reported that despite the lack of discernible downhole fractionation during LA, there is a potential 2–6% offset between *in situ* Lu–Hf ages and expected ages when using the non-matrix-matched NIST SRM 610 as the primary reference material. A

previous study found that such fractionation is not consistent and varies with instrument conditions.[46]

Matrix-induced elemental fractionations between NIST SRM 610, xenotime, apatite and garnet were investigated using a Photon Machines Analyte G2 + iCap TQ ICP-MS/MS system. There was no discernible downhole fractionation of Lu/Hf ratios during LA in any analytical sessions. MG-1 age data for 15 independent analytical sessions over 3 months are shown in Fig. 7 for calibrations by non-matrix-matched glass NIST SRM 610 and matrix-matched xenotime XN02. Xenotime MG-1 has been well-characterized by ID-TIMS U–Pb dating with a ^{206}Pb/^{238}U age of 490.0 ± 0.3 Ma.[24] Here, Lu–Hf ages of MG-1 xenotime calibrated against NIST SRM 610 ranged from 635 to 553 Ma with a corresponding matrix-bias (determined age/recommended age) of 1.13–1.30 (Fig. 7), whereas ages calibrated against XN02 xenotime were consistent and yielded a weighted-mean Lu–Hf age of 489.8 ± 2.2 Ma (MSWD = 0.6, n = 15), consistent with the ID-TIMS ^{206}Pb/^{238}U age.

We also found that the matrix-induced mass bias between NIST SRM 610 and MG-1 varied between sessions, so it is recommended that secondary matrix-matched reference materials should be used for calibration and quality-control purposes. The matrix-induced fractionation between NIST SRM 610 and apatite was examined using the Otter Lake and NW-1 apatite samples. The bias factors of Otter Lake and NW-1 between the NIST SRM 610 determined age and the recommended ages are 1.151 and 1.148, respectively, demonstrating the potential matrix effect between NIST SRM 610 and apatite samples. It is notable that the xenotimes analyzed in the same sessions with the aforementioned apatites have consistent bias factors of 1.150 (XN02) and 1.151 (Otter Lake), respectively, indicating that the xenotime and apatite have similar matrix effects to NIST SRM 610, so xenotime can be used as a reference material for *in situ* Lu–Hf dating of apatite. For garnet, the bias factors of 14SA36 and 15QL59 samples between the NIST SRM 610 determined age and the recommended ages are 1.051 and 1.049, respectively, which are obviously different from those (1.150) of XN02 xenotime, manifesting the potential matrix effect among NIST SRM 610, xenotime and garnet samples.

3.6 Analytical results

3.6.1 Xenotime. XN02 was analyzed as a matrix-matched reference material to correct for matrix-induced elemental fractionation of Lu–Hf ratios. The Lu–Hf age was normalized to the ID-TIMS U–Pb age,[23] so the accuracy of our technique could not be evaluated using this sample. A total of 246 spot analyses were undertaken in 20 analytical sessions over 3 months, 236 of which yielded a weighted-mean age of 515.4 ± 1.2 Ma (MSWD = 2.3; Fig. 8a). The uncertainties (2SE) of single-spot ages were ~2.6%. Calculated ^{176}Lu/^{177}Hf ratios ranged from 251 to 782 and ^{176}Hf/^{177}Hf ratios from 2.7 to 7.9. XN02 have relatively homogeneous Lu contents (median 5123 μg g^{-1}; ESI Table S1†). This sample has a median $f_{^{176}Hf}$ (the fraction of common ^{176}Hf) of 7.1%, so it is necessary to make common-Hf corrections to achieve accurate single-spot Lu–Hf ages.
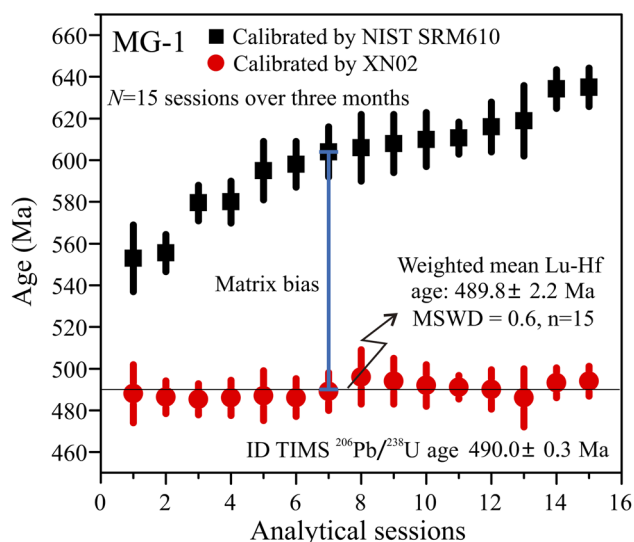

Fig. 7 Plot illustration of two-step calibration procedures for the *in situ* Lu–Hf geochronology. MG-1 ages calibrated by SRM 610 ranged from 545 to 630 Ma over 15 sessions in 3 months, illustrating that the matrix bias between SRM 610 and MG-1 may be dependent on instrument conditions. MG-1 data calibrated by XN02 were consistent with U–Pb ages, indicating the necessity of matrix calibration for *in situ* Lu–Hf geochronology.
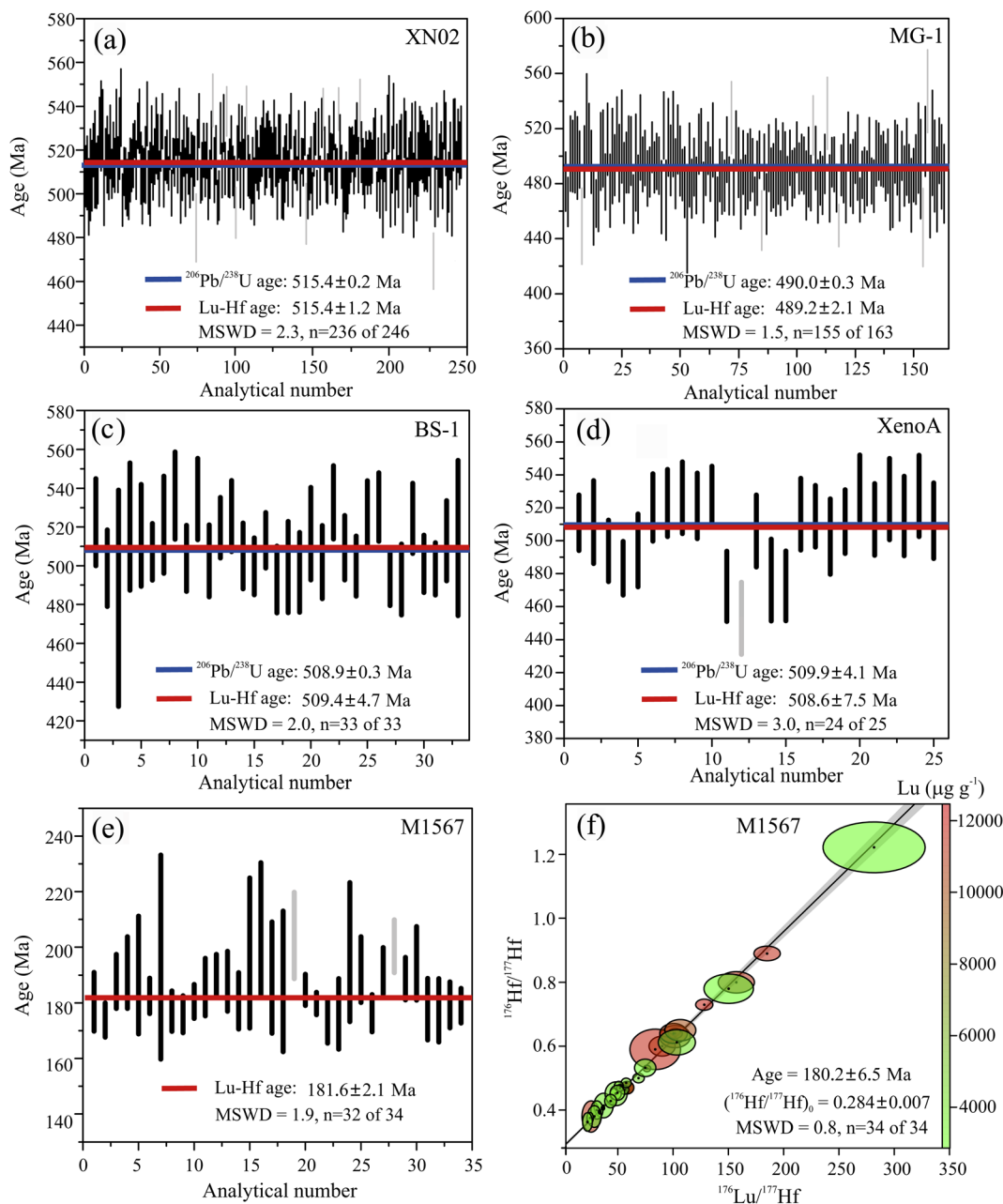
1294 | *J. Anal. At. Spectrom.*, 2023, **38**, 1285–1300

This journal is © The Royal Society of Chemistry 2023

Fig. 8 Common-Hf-corrected single-spot Lu–Hf ages of xenotimes XN02 (a), MG-1 (b), BS-1 (c), XenoA (d) and M1567 (e and f). M1567 contains an amount of common Hf, so the isochron age is plotted. Laser parameters were 50 μm spot size, 10 Hz frequency and 4.0 J cm^{-2}.

MG-1 was analyzed in 15 sessions, each including 15–20 analytical spots, over 3 months, with a total of 163 spot analyses. Lu–Hf ages were calculated using the matrix bias factor derived from XN02 xenotime, which was used for estimation of data accuracy of the calibration procedure. A total of 155 analyses yielded a weighted-mean age of 489.2 ± 2.2 Ma (MSWD = 1.5; Fig. 8b), consistent with the U–Pb age of 490.0 ± 0.3 Ma (ref. 24) within the analytical uncertainty. $^{176}Lu/^{177}Hf$ ratios ranged from 79 to 4130 and $^{176}Hf/^{177}Hf$ ratios ranged from 1.0 to 36.5. The relatively large single-spot age uncertainty (2SE) of ∼4.8% was due mainly to the relatively low Lu contents (median 851 μg g^{-1}; ESI Table S2†). The 15 weighted mean ages of 15 independent analytical sessions are consistent within ±1.5% uncertainty

(Fig. 8b). MG-1 has a variable $f_{^{176}Hf}$ of 0.6–28.1% (median 6.6%), so it was necessary to apply common-Hf corrections to obtain accurate single-spot Lu–Hf ages.

BS-1 was analyzed in one session, with a total of 33 spot analyses. Lu–Hf single-spot ages were plotted and are shown in Fig. 8c. The 33 analyses yielded a weighted-mean age of 509.4 ± 4.7 Ma (MSWD = 2.0; Fig. 8c), consistent with the U–Pb age of 508.9 ± 0.3 Ma (ref. 24). The single-spot age uncertainties (2SE) were ∼4.1%. The calculated $^{176}Lu/^{177}Hf$ ratios ranged from 280 to 755 and $^{176}Hf/^{177}Hf$ ratios from 2.9 to 7.8. BS-1 has variable Lu contents of ∼2000–5500 μg g^{-1} (ESI Table S3†). The sample has a median $f_{^{176}Hf}$ of 6.8%, which means common-Hf correction is required to obtain accurate single spot Lu–Hf ages.

This journal is © The Royal Society of Chemistry 2023

J. Anal. At. Spectrom., 2023, 38, 1285–1300 | 1295

XenoA was analyzed in one session, with a total of 25 spot analyses; the results are shown in Fig. 8d. A weighted-mean age of 508.6 ± 7.5 Ma (MSWD = 3.0; Fig. 8d) was obtained, consistent with the ID-TIMS U–Pb age. The uncertainties (2SE) of single spot ages were ~4.1%. The calculated $^{176}Lu/^{177}Hf$ ratios ranged from 1180 to 2306 and $^{176}Hf/^{177}Hf$ ratios, from 11 to 23. XenoA has relatively homogeneous Lu contents with a median of 2091 μg g^{-1} (ESI Table S4†). The sample has a median $f_{^{176}Hf}$ of 1.5%.

M1567 was analyzed in one session, with a total of 34 spot analyses. Plots of the common-Hf-corrected single spot ages and the Lu–Hf isochron ages are shown in Fig. 8e and f. A total of 34 analyses yielded an isochron age of 180.2 ± 6.5 Ma (MSWD = 0.8; Fig. 8f). The weighted mean common-Hf-corrected single-age is 181.6 ± 2.1 Ma (MSWD = 1.9; Fig. 8e). The calculated $^{176}Lu/^{177}Hf$ ratios ranged from 280 to 755 and $^{176}Hf/^{177}Hf$ ratios from 0.4 to 1.2 (ESI Table S5†). The sample has high $f_{^{176}Hf}$ values of 22.8–77.0% (median 59.0%). There is a lack of geochronological information for this sample, so the accuracy of our Lu–Hf age results for this sample could not be evaluated. However, the *in situ* Lu–Hf data may be judged reliably on the basis of the accuracy of analyses of quality control materials MG-1, BS-1 and XenoA.

3.6.2 Apatite. Otter Lake was analyzed in one session, with a total of 20 spot analyses. Data were corrected using XN02

xenotime as the primary reference material. Common-Hf-corrected single-spot ages are shown in Fig. 9a. The initial $^{176}Hf/^{177}Hf$ ratio of 0.284663 ± 0.000012 (collected from Otter Lake titanite[30]) was adopted for common-Hf correction. Here, $^{176}Lu/^{177}Hf$ and $^{176}Hf/^{177}Hf$ ratios were 63–359 and 1.5–7.0, respectively. Otter Lake apatite yielded a weighted-mean common-Hf-corrected single-spot age of 1038 ± 32 Ma (Fig. 9a), consistent with the solution Lu–Hf age (1031 ± 6 Ma) recorded by Barfod *et al.* (2005),[30] and *in situ* Lu–Hf age (1053 ± 12 Ma, n = 40, MSWD = 1.3) recorded by Simpson *et al.* (2021).[18] There is a strong decoupling between the U–Pb age (*ca.* 933 or *ca.* 913 Ma) and Lu–Hf age (*ca.* 1031 Ma) (Fig. 9d). These apatites are of hydrothermal origin and are found in a calcite (-rich) matrix. Some open system effect either in the U–Pb and/or Lu–Hf systems, or the simple cooling effect due to different closure temperatures could be responsible for this discrepancy. The Otter Lake sample has Lu contents of 4.6–10.9 μg g^{-1} (median 9.4 μg g^{-1}; ESI Table S6†), with a median $f_{^{176}Hf}$ of 9.9%.

NW-1 was analyzed in one session using a total of 20 spot analyses, and data were corrected using XN02 xenotime as the primary reference material. The initial $^{176}Hf/^{177}Hf$ ratio of 0.282 ± 0.004 was used for common-Hf correction, and the common-Hf-corrected single-spot ages are plotted in Fig. 9b. $^{176}Lu/^{177}Hf$ and $^{176}Hf/^{177}Hf$ ratios were 11.4–27.5 and 0.4–1.0, respectively, with a weighted-mean common-Hf-corrected single-spot age of
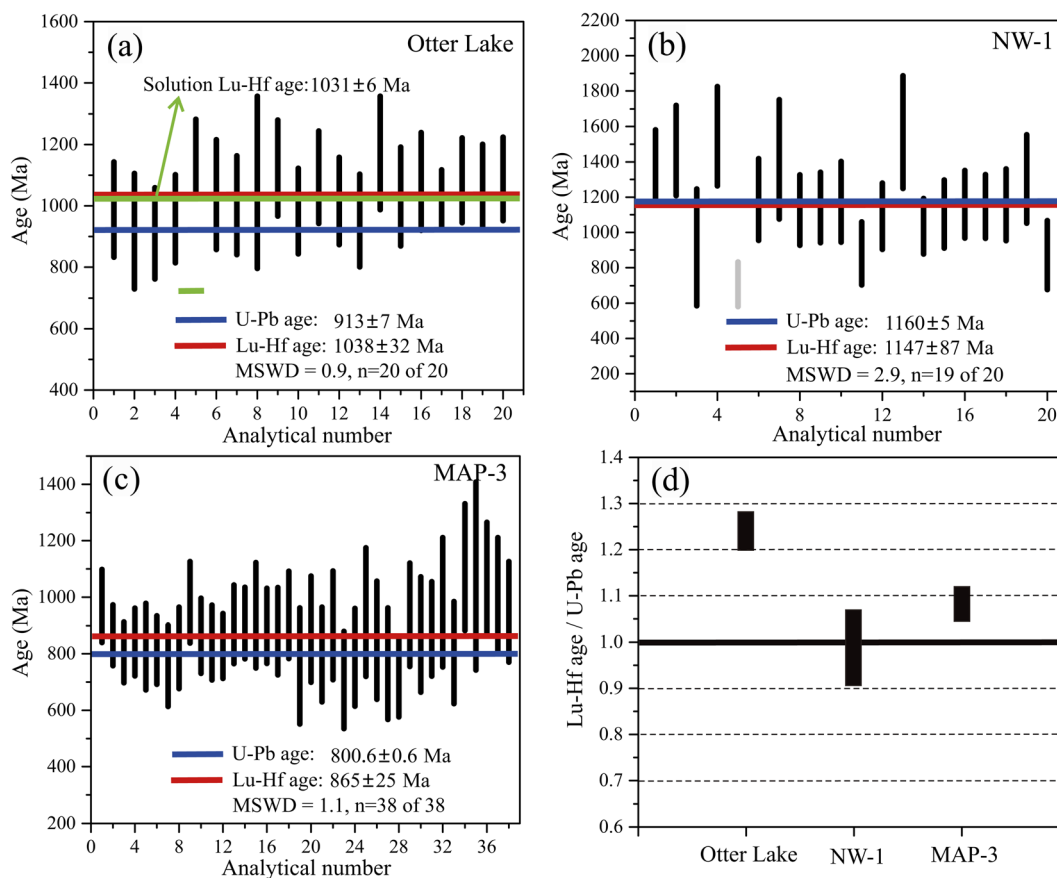

Fig. 9 Common-Hf-corrected single-spot Lu−Hf ages of apatites Otter Lake (a), NW-1 (b) and MAP-3 (c). U−Pb ages are plotted for comparison. The laser parameters were 120 μm spot size, 10 Hz frequency and 4.0 J cm^{-2}, except for NW-1 where the spot size was 90 μm due to limited sample sizes. (d) Plots of the ratios of Lu−Hf age and U−Pb age of three apatite samples.

1147 ± 87 Ma (Fig. 9b), consistent with the U–Pb age (1160 ± 6 Ma; Li *et al.* 2012 (ref. 28)). Lu contents ranged from ~2.9 to ~4.8 µg g^{-1}, with a median of 4.2 µg g^{-1}. The sample has a f_{176Hf} value of 30.5–55.1% (median 43.4%; ESI Table S7†).

MAP-3 was analyzed in one session using 37 spot analyses; data were corrected using XN02 xenotime as the primary reference material. Common-Hf corrected single-spot ages are plotted in Fig. 9c. The initial $^{176}Lu/^{177}Hf$ ratio of 0.282 ± 0.004 was used in the common-Hf correction. Owing to the low f_{176Hf} value (median 0.8%), $^{176}Lu/^{177}Hf$ and $^{176}Hf/^{177}Hf$ ratios could not be precisely determined. MAP-3 apatite yielded a weighted-mean single-spot age of 865 ± 25 Ma (Fig. 9c), older than the U–Pb age (800.6 ± 0.6 Ma; Duan *et al.* submitted;[31] Fig. 9d). The Lu contents of MAP-3 are relatively homogeneous, with a median of 5.7 µg g^{-1} (ESI Table S8†).

3.6.3 Garnet. 14SA36 was analyzed in one session using 73 spot analyses. Owing to a lack of matrix-matched Lu–Hf age reference materials, data were first corrected for instrument drift using NIST SRM 610, and then normalized to the meta-morphic zircon $^{207}Pb/^{206}Pb$ age of 3226.3 ± 5.5 Ma.[35] This sample has f_{176Hf} values of 4.9–99.9% (median 75.6%) and low and variable Lu contents of 0.02–4.17 µg g^{-1} (median 0.70 µg g^{-1}; ESI Table S9†). $^{176}Lu/^{177}Hf$ and $^{176}Hf/^{177}Hf$ ratios were between 0.02–68.6 and 0.28–4.35, respectively. The 73 spot analyses yielded an isochron age of 3207 ± 112 Ma (Fig. 10a). 14SA36 garnet yielded a weighted-mean common-Hf-corrected single-spot age of 3244 ± 33 Ma (Fig. 10b), based on the isochron intercept $^{176}Hf/^{177}Hf$ ratio.

12QL59 was analyzed in one session using 39 spot analyses. Lu–Hf ages were first corrected for instrument drift using NIST SRM 610, and then corrected for matrix-induced fractionation using a bias factor (1.051) derived from 14SA36 garnet. The sample has f_{176Hf} values of 33.3–100.9% (median 61.2%) and Lu contents of 0.7–5.4 µg g^{-1} (median 2.3 µg g^{-1}). $^{176}Lu/^{177}Hf$ and $^{176}Hf/^{177}Hf$ ratios were 0.8–69.0 and 0.29–0.95, respectively (ESI Table S10†). Thirty-eight spot analyses yielded an isochron age of 491.5 ± 50.6 Ma (Fig. 10c). The garnet yielded a weighted-mean common-Hf corrected single-spot age of 486.0 ± 12.9 Ma (Fig. 10d). The common-Hf corrected ages were based on the isochron intercept $^{176}Hf/^{177}Hf$ ratio.
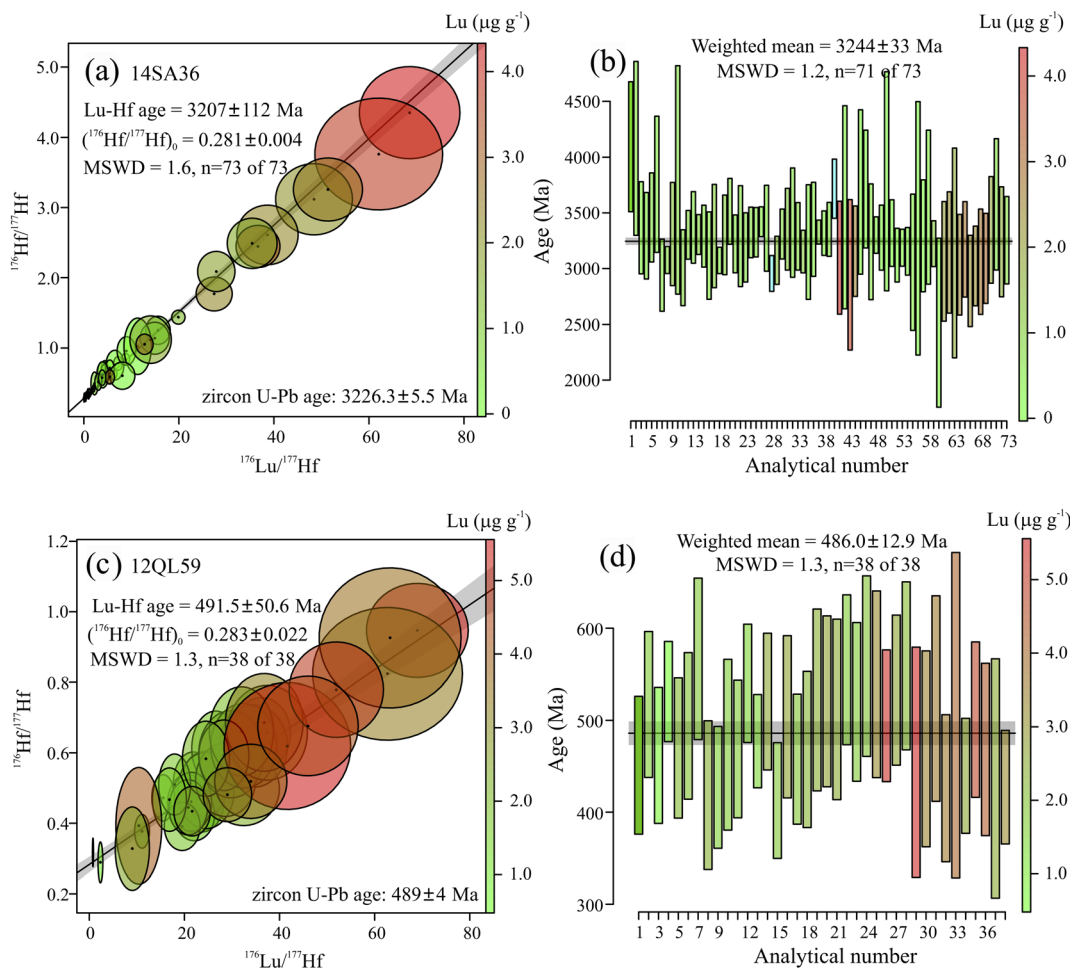

Fig. 10 Isochron and weighted-mean common-Hf-corrected single-spot ages of garnets 14SA36 (a and b) and 12QL59 (c and d). For 14SA36, data were first corrected for instrument drift using NIST SRM 610, and then normalized to the cogenetic zircon age ($^{207}Pb/^{206}Pb$ age: 3226.3 ± 5.5 Ma (ref. 33)). For 12QL59, the Lu–Hf age was first corrected for instrument drift using NIST SRM 610, and then corrected for matrix-induced fractionation using a bias factor (1.051) derived from 14SA36. The common-Hf corrected single-spot ages were made using isochron intercepts as the $^{176}Hf/^{177}Hf$-ratios.

3.7 Implications for *in situ* Lu–Hf dating

3.7.1 Lu contents and $f_{176_{Hf}}$ values. Lutetium contents and the $f_{176_{Hf}}$ values in the xenotime, apatite and garnet samples are plotted and shown in Fig. 11. Xenotime generally has high Lu and low common-Hf contents ($f_{176_{Hf}}$ values < 10%), so it is ideal for *in situ* Lu–Hf dating. U–Pb dating of xenotime is widely used as a robust and reliable dating method, and its *in situ* Lu–Hf dating may be an effective alternative geochronometer in the cases of low-U hydrothermal xenotime, or in dating complex xenotime grains with Pb-rich inclusions (*e.g.*, sulfides) that compromise the U–Pb dating methods. Apatite has low $f_{176_{Hf}}$ values and Lu contents (<10 μg g^{-1}), and large sampling volumes are needed (*e.g.*, laser spot size > 100 μm). Some apatites have very low Lu contents (<1.0 μg g^{-1}) as, for example, with the Mud Tank apatite (Lu: ∼0.26 μg g^{-1}), which means that not all apatites are suitable for *in situ* Lu–Hf dating. However, the closure temperature of the Lu–Hf system (675–750 °C) is higher than that of the U–Pb system (350–550 °C) for apatite. A promising avenue for future work would be to use U–Pb and Lu–Hf dating of apatite in tandem to more effectively track the timing and conditions of hydrothermal alteration or metamorphism of apatite-bearing rock samples. Garnet generally has variable $f_{176_{Hf}}$ values with low Lu contents (<5.0 μg g^{-1}), and enlarged sampling volumes are needed (*e.g.* laser spot size > 120 μm). We found some garnet crystals with very low Lu contents, and pre-screening (*e.g.*, 2D trace elemental imaging) for the high-Lu domains is necessary to ensure Lu–Hf dating success. In general, a laser spot size of 30–50 μm is sufficient for xenotime samples, while for apatite and garnet the laser spot size is >120 μm. The corresponding Lu concentrations are better higher than 5.0 μg g^{-1} for the samples with age < 1000 Ma and higher than 1.0 μg g^{-1} for the sample with age > 1000 Ma.

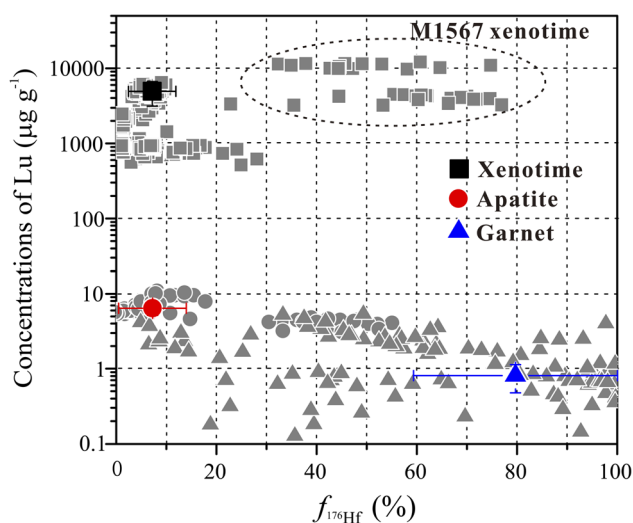**3.7.2 Accuracy and uncertainty.** Our xenotime Lu–Hf ages were consistent with the reported U–Pb ages within 1.5%

Fig. 11 Plot illustrating the $f_{176_{Hf}}$ values *vs.* Lu concentrations (μg g^{-1}). Xenotime samples included BS-1, MG-1, XN02, XENOA and M1567; apatite samples included Otter Lake, NM-1 and MAP-3; and garnet samples included 14SA35 and 12QL59. The median contents and proportion of common Hf were calculated and plotted.

uncertainty, demonstrating the reliability of the technique. The uncertainties of common-Hf corrected single-spot ages were in a range of 2.6–4.8% for the xenotime samples (Tables S1–S5†). The accuracy of Lu–Hf ages for apatite could not be estimated by comparison with U–Pb ages owing to the different closure temperatures of the two systems and the potential open system effect. However, based on comparison with the independent solution Lu–Hf age of the Otter Lake sample,[18] the accuracy was within analytical precision. For apatite samples, the uncertainties of common-Hf corrected single-spot ages were in a range of 9.2–36.0% (Tables S6–S8†). The relatively large uncertainties were due mainly to the low signal intensity of the radiogenic accumulated ^{176}Hf. For the garnet 12QL59 sample, thirty-eight spot analyses yielded an isochron age of 491.5 ± 50.6 Ma (Fig. 10c), which agreed well with the ^{206}Pb/^{238}U age of 489 ± 4 Ma obtained on metamorphic zircon. Moreover, the consistency between isochron and common-Hf corrected ages for samples 14SA36 and 12QL59 indicates that common-Hf-corrected ages might be particularly useful, with even a >50% common Hf component. However, only two garnets were analyzed in this study. The Lu–Hf age accuracy of 12QL59 garnet was validated using the matrix bias factor derived from 14SA36 garnet, but this needs to be confirmed using more samples with recommended ages. Our later work will be focused on this subject.

3.7.3 Development of reference materials. The investigated xenotime samples (XN02, BS-1, MG-1 and XenoA) may be useful as matrix-matched reference materials for *in situ* xenotime Lu–Hf analyses. For apatite, the Otter Lake apatite sample was the only apatite investigated here with a published Lu–Hf age of 1031 ± 6 Ma.[30] However, Simpson *et al.* (2021)[18] documented that this material may be too heterogeneous for Lu–Hf age determination. NW-1 is commonly used as an *in situ* U–Pb dating reference material, and our Lu–Hf age matched the U–Pb age well, so this material could be another candidate for use as an apatite Lu–Hf dating reference material. Currently, MAP-3 is characterized for the U–Pb age only by ID-TIMS, and it might be applicable as a Lu–Hf reference material after independent characterization using ID-MC-ICP-MS. Our study demonstrated that the xenotime reference materials can be used for apatite Lu–Hf dating. Lu–Hf reference materials for garnet are lacking, in particular for garnets having low common-Hf contents. It is always preferable that the low common-Hf content samples are used as the primary standards because of the less propagated uncertainties. Simpson *et al.* (2021)[18] documented that the Hogsbo garnet may be useful as a reference material for garnet age corrections. Garnet generally has variable $f_{176_{Hf}}$ values, which makes candidate selection difficult, and development of garnet Lu–Hf age reference materials for LA-ICP-MS/MS is a matter of urgency.

3.8 Comparison with an Agilent 8900 ICP-MS/MS

The main difference between the Thermal iCap TQ and Agilent 8900 systems is the design of the Q1 (the prefiltered quadruple). The iCap TQ instrument applies a short-length pole with high frequency to achieve a mass resolution of 1–10 amu, whereas the Agilent 8900 system applies one similar to Q3. For *in situ* Lu–

1298 | *J. Anal. At. Spectrom.*, 2023, **38**, 1285–1300

This journal is © The Royal Society of Chemistry 2023

Hf geochronology, the mass resolution of Q1 should be better than 1 amu to avoid the potential inference of $^{(175+83)}$Lu$^+$ on the $^{(176+82)}$Hf$^+$. Both instruments meet this requirement (1 amu mass resolution in Q1). Although instrument designs differ, the reaction products of Hf, Lu and Yb with NH$_3$ are very similar. For the iCap TQ ICP-MS instrument, high-purity NH$_3$ is more effective for the reaction than the commonly used 1:9 NH$_3$/He mixture. We found that the reaction rates of Yb ($\sim$0.00036%) for the iCap TQ ICP-MS was an order of magnitude higher than that of the Agilent 8900 ICP-MS/MS ($\sim$0.00003%). Currently, there is lack of sensitivity comparison between the Agilent 8900 ICP-MS/MS and iCap TQ ICP-MS/MS. Ideally, the sensitivity comparisons should involve the same LA system and homogeneous material. However, a higher sensitivity is always preferred,[18] particularly for low-Lu ($<$5.0 μg g^{-1}) garnet samples. Future work with sensitivity enhancement (*e.g.*, optimization of cone combinations) is anticipated.

4 Conclusions

Lu–Hf geochronology is a powerful method to constrain the temporal evolution of geological systems. In this study, an *in situ* Lu–Hf dating technique using LA-ICP-MS/MS was developed and successfully applied to a variety of Paleozoic–Precambrian xenotime, apatite and garnet. Several main conclusions were obtained in this work:

(1) For the iCap TQ ICP-MS/MS instrument, high-purity NH$_3$ is more effective in the reaction than the commonly used 1:9 NH$_3$/He mixture, and there was an 80% increase in sensitivity with an N$_2$ flow rate of 4.0 mL min^{-1}.

(2) Reaction products of Lu, Yb and Hf were identified in the mass range of 175–300 amu, with the product for separation of ^{176}Hf from ^{176}Lu and ^{176}Yb having mass +82. The reaction rates of Lu and Yb were $\sim$0.0034% and $\sim$0.00036%, respectively. Isobaric interferences ^{176}Lu and ^{176}Yb are required to correct for samples (*e.g.*, xenotime) with high ^{175}Lu/^{177}Hf and ^{172}Yb/^{177}Hf ratios.

(3) The matrix-induced bias in ^{176}Lu/^{177}Hf ratios between NIST SRM 610 and the samples requires further corrections using matrix-matched reference materials.

(4) Accurate Lu–Hf age results can be obtained for xenotime, apatite and garnet at a level of $<$1.5%, 2.5–7.5% and 3.5–10%, respectively. The analytical uncertainties could be further improved using a sensitivity-enhanced instrument and/or enlarged sampling volume.

Compared to the $<$10 analyses normally obtained during ID-TIMS, an important advantage of LA-ICP-MS/MS is the ability to quickly and easily obtain large, spatially resolved Lu–Hf geochronology datasets. Such large datasets are more easily interpretable in terms of isotopic disturbance and age mixing. The novel *in situ* Lu–Hf technique may be particularly useful in dating samples with complex growth records.

Author contributions

Shitou Wu conceived the study, conducted the experimental analyses, interpreted the data and wrote the initial manuscript; Hao Wang and Yueheng Yang led the project, conceived the study, interpreted the data and substantially edited the manuscript; Junlong Niu, Chao Huang, Liewen Xie, and Lei Xu provided technical support; Zhongwu Lan and Liangliang Zhang provided samples and revised the manuscript; Jinhui Yang and Fuyuang Wu interpreted the data and provided supervision; and all authors finalized the manuscript for publication.

Conflicts of interest

There are no conflicts of interest to declare.

Acknowledgements

References

1 E. Scherer, C. Münker and K. Mezger, *Science*, 2001, **293**, 683.

2 U. Söderlund, P. J. Patchett, J. D. Vervoort and C. E. Isachsen, *Earth Planet. Sci. Lett.*, 2004, **219**, 311–324.

3 P. J. Patchett and M. Tatsumoto, *Nature*, 1980, **288**, 571–574.

4 P. J. Patchett and M. Tatsumoto, *Contrib. Mineral. Petrol.*, 1981, **75**, 263–267.

5 J. Vervoort, *Encyclopedia of Scientific Dating Methods*, 2015, pp. 379–390.

6 D. Herwartz, T. J. Nagel, C. Münker, E. E. Scherer and N. Froitzheim, *Nat. Geosci.*, 2011, **4**, 178–183.

7 H. Cheng, R. L. King, E. Nakamura, J. D. Vervoort and Z. Zhou, *J. Metamorph. Geol.*, 2008, **26**, 741–758.

8 C. Münker, S. Weyer, E. Scherer and K. Mezger, *Geochem., Geophys., Geosyst.*, 2001, **2**, 1–19.

9 J. Blichert-Toft, C. Chauvel and F. Albarède, *Contrib. Mineral. Petrol.*, 1997, **127**, 248–260.

10 A. Schmidt, A. Pourteau, O. Candan and R. Oberhänsli, *Earth Planet. Sci. Lett.*, 2015, **432**, 24–35.

11 L. Tual, M. A. Smit, E. Cutts, E. Kooijman, M. Kielman-Schmitt, J. Majka and I. Foulds, *Chem. Geol.*, 2022, **607**, 121003.

12 G. Woods, *Agilent Application Note*. Agilent Technologies, Cheadle, 2016.

13 T. Zack and K. J. Hogmalm, *Chem. Geol.*, 2016, **437**, 120–133.

14 J. Hogmalm, T. Zack, A. K. O. Karlsson, A. S. L. Sjoqvist and D. Garbe-Schonberg, *J. Anal. At. Spectrom.*, 2017, **32**, 305–313.

15 K. J. Hogmalm, I. Dahlgren, I. Fridolfsson and T. Zack, *Miner. Deposita*, 2019, **54**, 821–828.

This journal is © The Royal Society of Chemistry 2023

J. Anal. At. Spectrom., 2023, **38**, 1285–1300 | **1299**

16 S. Gilbert and S. Glorie, *J. Anal. At. Spectrom.*, 2020, **35**, 1472–1481.

17 D. Xiang, Z. Zhang, T. Zack, D. Chew, Y. Yang, L. Wu and J. Hogmalm, *Geostand. Geoanal. Res.*, 2021, **45**, 621–642.

18 A. Simpson, S. Gilbert, R. Tamblyn, M. Hand, C. Spandler, J. Gillespie, A. Nixon and S. Glorie, *Chem. Geol.*, 2021, **577**, 120299.

19 D. A. Brown, A. Simpson, M. Hand, L. J. Morrissey, S. Gilbert, R. Tamblyn and S. Glorie, *Geology*, 2022, **50**, 837–842.

20 S. Seman, D. F. Stockli and N. M. McLean, *Chem. Geol.*, 2017, **460**, 106–116.

21 Y.-H. Yang, F.-Y. Wu, J.-H. Yang, R. H. Mitchell, Z.-F. Zhao, L.-W. Xie, C. Huang, Q. Ma, M. Yang and H. Zhao, *J. Anal. At. Spectrom.*, 2018, **33**, 231–239.

22 D. J. Cherniak, *Lithos*, 2006, **88**, 1–14.

23 A. Vasconcelos, G. Gonçalves, C. Lana, I. Buick, S. Kamo, F. Corfu, R. Scholz, A. Alkmim, G. Queiroga and H. Nalini Jr, *Geochem., Geophys., Geosyst.*, 2018, **19**, 2262–2282.

24 I. R. Fletcher, N. J. McNaughton, J. A. Aleinikoff, B. Rasmussen and S. L. Kamo, *Chem. Geol.*, 2004, **209**, 295–314.

25 D. M. Chew and R. A. Spikings, *Elements*, 2015, **11**, 189–194.

26 J. Gillespie, C. L. Kirkland, P. D. Kinny, A. Simpson, S. Glorie and K. Rankenburg, *Geochim. Cosmochim. Acta*, 2022, **338**, 121–135.

27 D. M. Chew, P. J. Sylvester and M. N. Tubrett, *Chem. Geol.*, 2011, **280**, 200–216.

28 Q.-L. Li, X.-H. Li, F.-Y. Wu, Q.-Z. Yin, H.-M. Ye, Y. Liu, G.-Q. Tang and C.-L. Zhang, *Gondwana Res.*, 2012, **21**, 745–756.

29 J. Thompson, S. Meffre, R. Maas, V. Kamenetsky, M. Kamenetsky, K. Goemann, K. Ehrig and L. Danyushevsky, *J. Anal. At. Spectrom.*, 2016, **31**, 1206–1215.

30 G. H. Barfod, E. J. Krogstad, R. Frei and F. Albarède, *Geochim. Cosmochim. Acta*, 2005, **69**, 1847–1859.

31 L.-J. Duan, L.-L. Zhang, D.-C. Zhu, Y.-H. Yang, J.-C. Xie, Q. Wang, S.-T. Wu, C. Huang, C. Li, W.-T. Xu, S. Kamo, J.-R. Tu, L.-J. Xu and G. Shi, *J. Anal. At. Spectrom.*, 2023, under review.

32 E. E. Scherer, K. L. Cameron and J. Blichert-Toft, *Geochim. Cosmochim. Acta*, 2000, **64**, 3413–3432.

33 M. A. Smit, E. E. Scherer and K. Mezger, *Earth Planet. Sci. Lett.*, 2013, **381**, 222–233.

34 X.-D. Deng, J.-W. Li, T. Luo and H.-Q. Wang, *Contrib. Mineral. Petrol.*, 2017, **172**, 71.

35 H. Wang, J. H. Yang, A. Kröner, Y. S. Zhu and R. Li, *Terra Nova*, 2019, **31**, 373–380.

36 Z. C. Hu, S. Gao, Y. S. Liu, S. H. Hu, H. H. Chen and H. L. Yuan, *J. Anal. At. Spectrom.*, 2008, **23**, 1093–1101.

37 S. Wu, M. Yang, Y. Yang, L. Xie, C. Huang, H. Wang and J. Yang, *Int. J. Mass Spectrom.*, 2020, **456**, 116394.

38 P. De Biévre and P. D. P. Taylor, *Int. J. Mass Spectrom. Ion Processes*, 1993, **123**, 149–166.

39 C. Paton, J. Hellstrom, B. Paul, J. Woodhead and J. Hergt, *J. Anal. At. Spectrom.*, 2011, **26**, 2508–2518.

40 O. Nebel, M. L. Morel and P. Z. Vroon, *Geostand. Geoanal. Res.*, 2009, **33**, 487–499.

41 P. Vermeesch, *Geosci. Front.*, 2018, **9**, 1479–1493.

42 D. Rösel and T. Zack, *Geostand. Geoanal. Res.*, 2022, **46**, 143–168.

43 S. Wu, G. Wörner, K. P. Jochum, B. Stoll, K. Simon and A. Kronz, *Geostand. Geoanal. Res.*, 2019, **43**, 567–584.

44 S. Wu, Y. Yang, K. P. Jochum, R. L. Romer, J. Glodny, I. P. Savov, S. Agostini, J. C. M. De Hoog, S. T. M. Peters, A. Kronz, C. Zhang, Z. Bao, X. Wang, Y. Li, G. Tang, L. Feng, H. Yu, Z. Li, Z. Le, J. Lin, Y. Zeng, C. Xu, Y. Wang, Z. Cui, L. Deng, J. Xiao, Y. Liu, D. Xue, Z. Di, L. Jia, H. Wang, L. Xu, C. Huang, L. Xie, A. Pack, G. Wörner, M. He, C. Li, H. Yuan, F. Huang, Q. Li, J. Yang, X. Li and F. Wu, *Geostand. Geoanal. Res.*, 2021, **45**, 719–745.

45 P. J. Sylvester, *Laser Ablation ICP-MS in the Earth Sciences: Current Practices and Outstanding Issues*, ed. P. Sylvester, Mineralogical Association of Canada. Short Course Series, 2008, vol. 40, pp. 67–78.

46 S. Wu, Y. Yang, N. M. W. Roberts, M. Yang, H. Wang, Z. Lan, B. Xie, T. Li, L. Xu, C. Huang, L. Xie, J. Yang and F. Wu, *Sci. China Earth Sci.*, 2022, **65**, 1146–1160.

1300 | *J. Anal. At. Spectrom.*, 2023, **38**, 1285–1300

This journal is © The Royal Society of Chemistry 2023